A&A 580, A22 (2015)
DOI: 10.1051/0004-6361/201424496

Astronomy & Astrophysics

Planck intermediate results

XXIV. Constraints on variations in fundamental constants⋆

Planck Collaboration: P. A. R. Ade[73], N. Aghanim[50], M. Arnaud[62], M. Ashdown[59,5], J. Aumont[50], C. Baccigalupi[72], A. J. Banday[80,9], R. B. Barreiro[56], E. Battaner[81,82], K. Benabed[51,79], A. Benoit-Lévy[21,51,79], J.-P. Bernard[80,9], M. Bersanelli[29,42], P. Bielewicz[80,9,72], J. R. Bond[8], J. Borrill[12,75], F. R. Bouchet[51,79], C. Burigana[41,27], R. C. Butler[41], E. Calabrese[77], A. Chamballu[62,14,50], H. C. Chiang[24,6], P. R. Christensen[69,32], D. L. Clements[47], L. P. L. Colombo[20,57], F. Couchot[60], A. Curto[5,56], F. Cuttaia[41], L. Danese[72], R. D. Davies[58], R. J. Davis[58], P. de Bernardis[28], A. de Rosa[41], G. de Zotti[38,72], J. Delabrouille[1], J. M. Diego[56], H. Dole[50,49], O. Doré[57,10], X. Dupac[35], T. A. Enßlin[66], H. K. Eriksen[54], O. Fabre[51], F. Finelli[41,43], O. Forni[80,9], M. Frailis[40], E. Franceschi[41], S. Galeotta[40], S. Galli[51], K. Ganga[1], M. Giard[80,9], J. González-Nuevo[56,72], K. M. Górski[57,83], A. Gregorio[30,40,45], A. Gruppuso[41], F. K. Hansen[54], D. Hanson[67,57,8], D. L. Harrison[53,59], S. Henrot-Versillé[60], C. Hernández-Monteagudo[11,66], D. Herranz[56], S. R. Hildebrandt[10], E. Hivon[51,79], M. Hobson[5], W. A. Holmes[57], A. Hornstrup[15], W. Hovest[66], K. M. Huffenberger[22], A. H. Jaffe[47], W. C. Jones[24], E. Keihänen[23], R. Keskitalo[12], R. Kneissl[34,7], J. Knoche[66], M. Kunz[16,50,2], H. Kurki-Suonio[23,37], J.-M. Lamarre[61], A. Lasenby[5,59], C. R. Lawrence[57], R. Leonardi[35], J. Lesgourgues[78,71], M. Liguori[26], P. B. Lilje[54], M. Linden-Vørnle[15], M. López-Caniego[56], P. M. Lubin[25], J. F. Macías-Pérez[64], N. Mandolesi[41,4,27], M. Maris[40], P. G. Martin[8], E. Martínez-González[56], S. Masi[28], S. Matarrese[26], P. Mazzotta[31], P. R. Meinhold[25], A. Melchiorri[28,44], L. Mendes[35], E. Menegoni[63], A. Mennella[29,42], M. Migliaccio[53,59], M.-A. Miville-Deschênes[50,8], A. Moneti[51], L. Montier[80,9], G. Morgante[41], A. Moss[74], D. Munshi[73], J. A. Murphy[68], P. Naselsky[69,32], F. Nati[28], P. Natoli[27,3,41], H. U. Nørgaard-Nielsen[15], F. Noviello[58], D. Novikov[47], I. Novikov[69], C. A. Oxborrow[15], L. Pagano[28,44], F. Pajot[50], D. Paoletti[41,43], F. Pasian[40], G. Patanchon[1], O. Perdereau[60], L. Perotto[64], F. Perrotta[72], F. Piacentini[28], M. Piat[1], E. Pierpaoli[20], D. Pietrobon[57], S. Plaszczynski[60], E. Pointecouteau[80,9], G. Polenta[3,39], N. Ponthieu[50,46], L. Popa[52], G. W. Pratt[62], S. Prunet[51,79], J. P. Rachen[18,66], R. Rebolo[55,13,33], M. Reinecke[66], M. Remazeilles[58,50,1], C. Renault[64], S. Ricciardi[41], I. Ristorcelli[80,9], G. Rocha[57,10,⋆⋆], G. Roudier[1,61,57], B. Rusholme[48], M. Sandri[41], G. Savini[70], D. Scott[19], L. D. Spencer[73], V. Stolyarov[5,59,76], R. Sudiwala[73], D. Sutton[53,59], A.-S. Suur-Uski[23,37], J.-F. Sygnet[51], J. A. Tauber[36], D. Tavagnacco[40,30], L. Terenzi[41], L. Toffolatti[17,56], M. Tomasi[29,42], M. Tristram[60], M. Tucci[16,60], J.-P. Uzan[51,79], L. Valenziano[41], J. Valiviita[23,37], B. Van Tent[65], P. Vielva[56], F. Villa[41], L. A. Wade[57], D. Yvon[14], A. Zacchei[40], and A. Zonca[25]

(Affiliations can be found after the references)

Received 29 June 2014 / Accepted 21 November 2014

ABSTRACT

Any variation in the fundamental physical constants, more particularly in the fine structure constant, α, or in the mass of the electron, m_e, affects the recombination history of the Universe and cause an imprint on the cosmic microwave background angular power spectra. We show that the *Planck* data allow one to improve the constraint on the time variation of the fine structure constant at redshift $z \sim 10^3$ by about a factor of 5 compared to WMAP data, as well as to break the degeneracy with the *Hubble* constant, H_0. In addition to α, we can set a constraint on the variation in the mass of the electron, m_e, and in the simultaneous variation of the two constants. We examine in detail the degeneracies between fundamental constants and the cosmological parameters, in order to compare the limits obtained from *Planck* and WMAP and to determine the constraining power gained by including other cosmological probes. We conclude that independent time variations of the fine structure constant and of the mass of the electron are constrained by *Planck* to $\Delta\alpha/\alpha = (3.6 \pm 3.7) \times 10^{-3}$ and $\Delta m_e/m_e = (4 \pm 11) \times 10^{-3}$ at the 68% confidence level. We also investigate the possibility of a spatial variation of the fine structure constant. The relative amplitude of a dipolar spatial variation in α (corresponding to a gradient across our *Hubble* volume) is constrained to be $\delta\alpha/\alpha = (-2.4 \pm 3.7) \times 10^{-2}$.

Key words. cosmology: observations – cosmic background radiation – cosmological parameters – atomic data

1. Introduction

The construction of the standard cosmological model, known as Λ cold dark matter (ΛCDM), relies on the assumption that general relativity offers a good description of gravity on astrophysical scales. The existence of a dark sector, including both dark matter and dark energy, has motivated an important activity in testing general relativity on astrophysical scales (see, Uzan 2007; Jain et al. 2013, for reviews) in order to better quantify and extend its domain of validity. As part of this programme, testing for the constancy of fundamental constants offers a unique window on the Einstein equivalence principle (see Dicke 1964 and Uzan 2003, 2011 for reviews) and thus on general relativity, as well as on other metric theories of gravity.

Various systems, spanning different time scales and physical environments, are now used to set constraints on a possible variation in the fundamental constants. This includes the comparison of atomic clocks in the laboratory at $z = 0$ (Rosenband et al. 2008; Cingöz et al. 2008; Peik et al. 2008; Bize et al. 2003), the Oklo phenomenon at a redshift $z \simeq 0.14$

⋆ Appendices are available in electronic form at http://www.aanda.org

⋆⋆ Corresponding author: Graca Rocha, e-mail: graca.m.rocha@jpl.nasa.gov

Table 1. Summary of the 68% confidence limit (CL) bounds on the variation of fundamental constants obtained from previous analyses of cosmological data and more particularly of CMB data.

Constraint ($\alpha \times 10^2$)	Data	Other parameters	Reference
$[-9, 2]$	COBE-BOOMERanG-DASI + BBN	BBN with α only	(Avelino et al. 2001)
		$(\Omega_c, \Omega_b, h, n_s)$	
$[-1.4, 2]$	COBE-BOOMERanG-MAXIMA	$(\Omega_c, \Omega_b, h, n_s)$	(Landau et al. 2001)
$[-5, 2]$	WMAP-1	$(\Omega_c h^2, \Omega_b h^2, \Omega_\Lambda h^2, \tau, n_s, \mathrm{d}n_s/\mathrm{d}\ln k)$	(Rocha et al. 2004)
$[-6, 1]$	WMAP-1	Same as above + $\mathrm{d}n_s/\mathrm{d}\ln k = 0$	(Rocha et al. 2004)
$[-9.7, 3.4]$	WMAP-1	$(\Omega_c, \Omega_b, h, n_s, \tau, m_e)$	(Ichikawa et al. 2006)
$[-4.2, 2.6]$	WMAP-1 + HST	$(\Omega_c, \Omega_b, h, n_s, \tau, m_e)$	(Ichikawa et al. 2006)
$[-3.9, 1.0]$	WMAP-3 (TT, TE, EE) + HST	$(\Omega_c, \Omega_b, h, n_s, z_{re}, A_s)$	(Stefanecsu 2007)
$[-1.2, 1.8]$	WMAP-5 + ACBAR + CBI + 2df	$(\Omega_c h^2, \Omega_b h^2, \Theta_*, \tau, n_s, A_s, m_e)$	(Scoccola et al. 2008)
$[-1.9, 1.7]$	WMAP-5 + ACBAR + CBI + 2df	$(\Omega_c h^2, \Omega_b h^2, \Theta_*, \tau, n_s, A_s, m_e)$	(Scoccola et al. 2009)
$[-5.0, 4.2]$	WMAP-5 + HST	$(\Omega_c h^2, \Omega_b h^2, h, \tau, n_s, A_s)$	(Nakashima et al. 2008)
$[-4.3, 3.8]$	WMAP-5 + ACBAR + QUAD + BICEP	$(\Omega_c h^2, \Omega_b h^2, h, \tau, n_s)$	(Menegoni et al. 2009)
$[-1.3, 1.5]$	WMAP-5 + ACBAR + QUAD + BICEP + HST	$(\Omega_c h^2, \Omega_b h^2, h, \tau, n_s)$	(Menegoni et al. 2009)
$[-0.83, 0.18]$	WMAP-5 (TT, TE, EE)	$(\Omega_c h^2, \Omega_b h^2, h, \tau, n_s, A_s, m_e, \mu)$	(Nakashima et al. 2010)
$[-2.5, -0.3]$	WMAP-7 + H_0 + SDSS	$(\Omega_c h^2, \Omega_b h^2, \Theta_*, \tau, n_s, A_s, m_e)$	(Landau & Scóccola 2010)

Notes. All assume $\Omega_K = 0$, i.e., no spatial curvature. Here Ω_b, Ω_c, and Ω_Λ refer to the density parameters for the baryons, cold dark matter, and cosmological constant, respectively. In addition h is the reduced Hubble constant, τ the reionization optical depth, Θ_* the angular size of the sound horizon at last scattering, and the spectrum of the initial curvature perturbation is characterized by an amplitude A_s, a spectral index n_s and potentially a running, $\mathrm{d}n_s/\mathrm{d}\ln k$. For comparison, our new analysis, based on the *Planck* data, uses $(\Omega_c h^2, \Omega_b h^2, H_0, \tau, n_s, A_s, \alpha, m_e)$.

(Kuroda 1956; Shlyakhter 1976; Damour & Dyson 1996; Fujii et al. 2000a; Gould et al. 2006), meteorite dating (Wilkinson 1958; Dyson 1972; Fujii et al. 2000a; Olive et al. 2002), quasar absorption spectra observations (Savedoff 1956; Webb et al. 2001; Srianand et al. 2004, 2007), molecular absorption lines (Carilli et al. 2001; Kanekar et al. 2005), clusters of galaxies (Galli 2013), population III stars (Livio et al. 1989; Ekström et al. 2010; Coc et al. 2009), cosmic microwave background (CMB) anisotropies (see below for details), and big bang nucleosynthesis at $z \sim 10^8$ (Bergström et al. 1999; Müller et al. 2004; Coc et al. 2007, 2012). Several reviews (e.g., Uzan 2003, 2011; Martins 2003; Flambaum 2007) provide detailed discussions of the various methods and constraints. The claim that the fine structure constant may have been smaller in the past (Webb et al. 2001), drawn from observations of specific quasar absorption spectra by the Keck telescope, has not been confirmed by independent studies. All VLT observations of quasar absorption spectra (Srianand et al. 2004, 2007) and observations of molecular absorption lines (Kanekar et al. 2005), are compatible with no variation (see also Bonifacio et al. 2014, and references therein). Despite the lack of definitive empirical evidence of any constants having a different value in the past, there are many theoretical ideas to motivate the continued search for variations in cosmological data.

The observation of CMB temperature anisotropies has been used extensively to constrain the variation in fundamental constants at a redshift $z \simeq 10^3$. Earlier analyses relied on the data from BOOMERanG and MAXIMA (Kaplinghat et al. 1999; Avelino et al. 2000; Landau et al. 2001) and on the WMAP data combined with other cosmological probes (Rocha et al. 2004; Martins et al. 2004b,a; Ichikawa et al. 2006; Stefanecsu 2007; Scoccola et al. 2008; Nakashima et al. 2008; Menegoni et al. 2009; Menegoni 2010), first focusing on the effect of a variation in the fine structure constant alone (Rocha et al. 2004; Martins et al. 2004b; Stefanecsu 2007; Nakashima et al. 2008, 2010; Menegoni et al. 2009; Landau & Scóccola 2010), and then also including a possible variation in the electron mass (Ichikawa et al. 2006; Scoccola et al. 2008, 2009; Nakashima et al. 2010; Landau & Scóccola 2010; Scóccola et al. 2013). Such studies typically indicate that, on cosmological scales, these two parameters are constant at the percent level. The previous constraints and the set of cosmological parameters used to perform the analyses are summarized in Table 1.

From a physical point of view, the effects of a variation in the fundamental constants on the CMB are mostly caused by the modifications to the recombination process. As first discussed in Hannestad (1999), a variation in the fine structure constant can be implemented in the `RECFAST` code (Seager et al. 1999), but one should also include the variation in the mass of the electron (Battye et al. 2001) or, equivalently, the electron-to-proton mass ratio. In this new study, we implement a possible variation in the fundamental constants in a modified version of `RECFAST`, as used in earlier works (Avelino et al. 2001; Rocha et al. 2004; Martins et al. 2004b; Scoccola et al. 2008).

The shape of the CMB power spectrum depends on the cosmological parameters and, as we see in Sect. 3, there exist degeneracies between the fundamental constants and these cosmological parameters. Previous studies (see e.g., Table 1 for concrete examples) have, at the percent level, constrained the variation of the fundamental constants between the time of recombination and today. As we show, the resolution of the *Planck* data allows us to break some of the degeneracies and to improve these constraints. They can be further enhanced by combining CMB data with other cosmological probes (see Table 1).

The goal of the present study is to constrain the variation in the fundamental constants using the recent *Planck*[1] data

[1] *Planck* (`http://www.esa.int/Planck`) is a project of the European Space Agency (ESA) with instruments provided by two scientific consortia funded by ESA member states (in particular the lead countries, France and Italy) with contributions from NASA (USA), and telescope reflectors provided in a collaboration between ESA and a scientific consortium led and funded by Denmark.

(Planck Collaboration I 2014). We start by considering only a time variation of the fine structure constant. This analysis extends the one presented in Planck Collaboration XVI (2014) by showing the effect of combining the *Planck* data with a number of additional data sets. We then discuss the time variation of the mass of the electron and the simultaneous time variation of these two constants. Furthermore, we address the possibility of a spatial dependence by the fine structure constant.

The article is organized as follows. We start by discussing the phenomenological implementation of the physics that depends on the fundamental constants in Sect. 2. Section 3 focuses on a pure (spatially homogeneous) time variation of the fine structure constant or of the mass of the electron, assuming that all other constants remain strictly constant. Section 4 considers the case in which both constants are allowed to vary. Section 5 investigates the possibility of a spatial variation, focusing on a dipolar modulation of the fine structure constant on the sky. It is first shown that such a variation induces mode coupling between the $a_{\ell m}$, which can then be constrained. We summarize the constraints in Sect. 6 and also discuss extensions and limitations of our approach. Technical details of the effects on the recombination process are summarized in Appendix A, while Appendix B provides an in-depth description of the difference between a variation in α and a variation in m_e.

It is worth making some preparatory statements about notation. We generically represent the set of constants by c_p. We denote the CMB temperature anisotropy observed in the direction $\hat{\boldsymbol{n}}$ by either $\bar{\Theta}(\hat{\boldsymbol{n}})$ or $\Theta(\hat{\boldsymbol{n}}\,; c_p)$, the former assuming that it is evaluated using the current values of the fundamental constants as determined by laboratory experiments, $\bar{\Theta}(\hat{\boldsymbol{n}}) \equiv \Theta(\hat{\boldsymbol{n}}\,; c_{p,0})$. These can both be expanded in terms of spherical harmonics as

$$\bar{\Theta}(\hat{\boldsymbol{n}}) = \sum_{\ell m} \bar{a}_{\ell m} Y_{\ell m}(\hat{\boldsymbol{n}}), \tag{1}$$

and similarly for Θ, with multipolar coefficients $a_{\ell m}$. We define the angular power spectrum as usual by

$$(2\ell+1)\bar{C}_\ell \equiv \sum_m \langle \bar{a}_{\ell m} \bar{a}^*_{\ell m} \rangle. \tag{2}$$

Statistical homogeneity and isotropy imply that $\langle \bar{a}_{\ell m} \bar{a}_{\ell' m'} \rangle = \bar{C}_\ell \delta_{\ell\ell'} \delta_{mm'}$. However, this property has no general reason to hold, in particular when we consider a possible spatial variation of the fundamental constants (see Sect. 5).

The physics of recombination is mostly determined by the atomic physics of hydrogen and helium, and in principle, depends on the fine structure constant

$$\alpha \equiv \frac{\mathrm{e}^2}{4\pi\varepsilon_0 \hbar c}, \tag{3}$$

the masses of the electron and of the proton, m_e and m_p; the proton gyromagnetic factor, g_p; and the gravitational constant, G, which enters through the expansion dynamics and the Friedmann equation. As explained in Sect. 2.1, the effect of a variation in m_p on recombination is subdominant compared to a variation in m_e, while g_p enters only into the hyperfine structure, which is not relevant for the recombination process. In this paper, we assume that G is kept fixed, so one could consider that a variation of m_e actually corresponds to a variation in the dimensionless quantity $Gm_\mathrm{e}^2/\hbar c$ (however, see the discussion in Sect. 2.2).

2. Implementation of the variation of fundamental constants

The main effect of a variation of the fundamental constants is to induce a modification of the recombination rates that are mostly dependent on the fine structure constant and on the electron mass. These two constants are thus our primary focus and we summarize their impact on the recombination process in Sect. 2.1. However, assuming that a mass may be dynamical requires us to specify the model further, since we can imagine, e.g., that all the masses are varying while keeping their ratios constant, or that the mass ratios are varying. We briefly discuss these possibilities in Sect. 2.2.

2.1. Modification of the recombination dynamics

CMB angular power spectra strongly depend on the time and width of last scattering, i.e., on when and how photons decoupled from electrons. This information is encoded in the visibility function, which quantifies the probability distribution that a photon last scatters at a certain conformal time η, and is defined as

$$g(\eta)\mathrm{d}\eta = \dot{\tau}\mathrm{e}^{-\tau}\mathrm{d}\eta, \tag{4}$$

where $\tau = \int \dot{\tau}\mathrm{d}\eta$ is the optical depth and $\dot{\tau}$ is the Thomson scattering rate:

$$\dot{\tau} = n_\mathrm{e} c \sigma_\mathrm{T} a. \tag{5}$$

Here n_e is the number density of free electrons, c the speed of light, a the scale factor, and σ_T the Thomson scattering cross-section. A change in the fundamental constants modifies the Thompson scattering rate $\dot{\tau}$ (and thus the visibility function) in a number of different ways. First, the Thomson scattering cross-section is given by

$$\sigma_\mathrm{T} = \frac{8\pi}{3}\frac{\hbar^2}{m_\mathrm{e}^2 c^2}\alpha^2. \tag{6}$$

A variation of the fundamental constants implies that

$$\sigma_\mathrm{T} = \sigma_{\mathrm{T}0}\left(\frac{\alpha}{\alpha_0}\right)^2\left(\frac{m_\mathrm{e}}{m_{\mathrm{e}0}}\right)^{-2}. \tag{7}$$

Second, a change in fundamental constants modifies the equations determining the evolution with time of the free electron fraction x_e. The free electron fraction can be determined as the sum of the free proton fraction x_p and of the singly ionized helium fraction x_He, whose evolution can be calculated by solving the system of differential equations summarized in Appendix A, together with the evolution of the matter temperature T_M (see, e.g., Seager et al. 1999). These equations involve a series of quantities that have to be modified when assuming a variation of the fundamental constants. We will describe the most important dependences below.

Since the energy levels scale as $B_\mathrm{i} \propto \alpha^2 m_\mathrm{e}$, it follows that the transition frequencies behave as

$$\nu_\mathrm{i} = \nu_{\mathrm{i}0}\left(\frac{\alpha}{\alpha_0}\right)^2\left(\frac{m_\mathrm{e}}{m_{\mathrm{e}0}}\right), \tag{8}$$

where any quantity with a subscript "0" has to be understood to be evaluated with its standard value, as known experimentally (see, e.g., Mohr et al. 2008). We note that it is in fact the reduced mass $m_\mathrm{r} = m_\mathrm{e}M/(m_\mathrm{e}+M)$, M being the mass of the nucleus,

which should appear in the transition frequencies, but clearly at lowest order $\delta m_r/m_r = \delta m_e/m_e(1 + m_e/M) \simeq \delta m_e/m_e$. This explains why the dependency is in m_e and not m_r. Note also that the gyromagnetic factor does not enter in the dipolar transitions or in the energies, so that it does not enter the discussion at all.

The photoionization cross-sections all scale as $\alpha^{-1}m_e^{-2}$, so that

$$\sigma_n = \sigma_{n0}\left(\frac{\alpha}{\alpha_0}\right)^{-1}\left(\frac{m_e}{m_{e0}}\right)^{-2}. \quad (9)$$

The recombination coefficient $\widetilde{\alpha}_i$ scales as[2] $\alpha^3 m_e^{-3/2}$, so that

$$\widetilde{\alpha}_i = \widetilde{\alpha}_{i0}\left(\frac{\alpha}{\alpha_0}\right)^{3}\left(\frac{m_e}{m_{e0}}\right)^{-3/2}. \quad (10)$$

The ionization coefficient can then be defined as $\beta_i = \widetilde{\alpha}_i(2\pi m_e kT_M/h^2)^{3/2}\exp(-h\nu_i/kT_M)$, so that it scales as

$$\beta_i = \beta_{i0}\left(\frac{\alpha}{\alpha_0}\right)^{3}\exp(-h\nu_i/kT_M), \quad (11)$$

where the frequency ν_i depends on the constants as in Eq. (8). The "K-factors" (see Appendix A for definition) account for the cosmological redshifting of the photons, and scale as

$$K_i = K_{i0}\left(\frac{\alpha}{\alpha_0}\right)^{-6}\left(\frac{m_e}{m_{e0}}\right)^{-3}. \quad (12)$$

To finish, the Einstein A coefficient scales as $\alpha^5 m_e$ and the two-photon decay rates as $\alpha^8 m_e$, so that

$$A_i = A_{i0}\left(\frac{\alpha}{\alpha_0}\right)^{5}\left(\frac{m_e}{m_{e0}}\right), \quad \Lambda_i = \Lambda_{i0}\left(\frac{\alpha}{\alpha_0}\right)^{8}\left(\frac{m_e}{m_{e0}}\right). \quad (13)$$

We incorporate all these modifications in the code RECFAST (Seager et al. 1999; Seager et al. 2000), so that the impact of a variation of the fundamental constants on recombination can be inferred. In the following, we impose the condition that the value of the constants can differ from the standard ones only at redshifts higher than around 50[3], and we consistently include variations both for hydrogen and helium recombination physics.

[2] The scaling of the effective recombination coefficient with the fine structure constant is not clearly established; throughout the paper we assume it to be cubic, following the scaling for the rates between individual atomic levels. However, there have been other suggested scalings published, e.g., Narimani et al. (2012) adopted α^5, while Kaplinghat et al. (1999) suggested a scaling motivated by the dependence of the effective recombination rate on temperature, yielding $\alpha^{3.4}$. We checked however that this difference in scaling has a subdominant impact on the spectra and that the results are essentially unmodified, whichever scaling we choose.

[3] It is assumed that the constants do not vary on a time scale approximately the width of the last scattering surface. As long as matter and radiation are tightly coupled, the equation of evolution of the distribution of the photons after decoupling, is described by a Liouville equation, instead of a Boltzmann equation, so that neither α nor m_e enter the discussion. Thus, we actually implicitly assume that the constants relax to their current value before reionization, i.e., before about $z = 10$. The dynamics of this relaxation is indeed model-dependent, but the constraints at lower redshifts suggest that the variation between redshifts around 4 and today has to be smaller than 10^{-5}. Any relaxation dynamics of the constants from their values at the epoch of recombination to their laboratory ones will not affect the analysis as long as it takes place after recombination and before the reionization era. In any case, we are essentially assuming that there is one value at the recombination epoch and another value today.

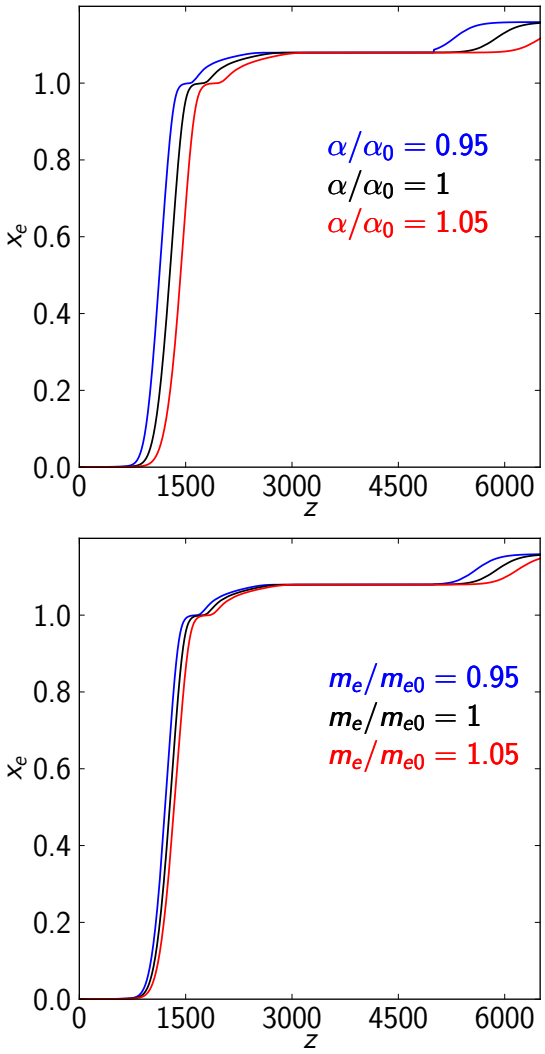

Fig. 1. Evolution of the free electron fraction x_e with redshift z for different values of the fine structure constant α (*top*) and of the mass of the electron (*bottom*). The coloured lines refer to a −5% (blue) and +5% (red) variation of the constants, while the black line shows the standard case. The decreases at redshift around 6000 and 2000 correspond to the first and second recombination of helium, while the large decrease at redshift 1300 is due to the recombination of hydrogen.

Figure 1 shows the evolution of the free electron fraction $x_e(z)$ with redshift under a relative variation of ±5% of either the fine structure constant, α, or of the mass of the electron, m_e. As can be noticed, a larger value of either of the two constants shifts the recombination epoch to earlier times, i.e., to higher redshifts. The effect is stronger for α than for m_e, mainly because of the different dependence of the transition frequencies on the two constants (see Eq. (8)). A detailed explanation of how the different dependences listed in this section affect the dynamics of recombination is reported in Appendix B.

Figure 2 shows the effect of a variation in α or m_e on the CMB angular power spectra (temperature, EE polarization and TE cross-correlation). For a larger value of the constants, recombination happens earlier, resulting in three main effects on the power spectra.

The first effect is that the sound horizon at recombination is smaller, and the angular diameter distance to the last scattering surface is larger. As a consequence, the positions of the acoustic peaks shift to higher multipoles, in a way that can be degenerate

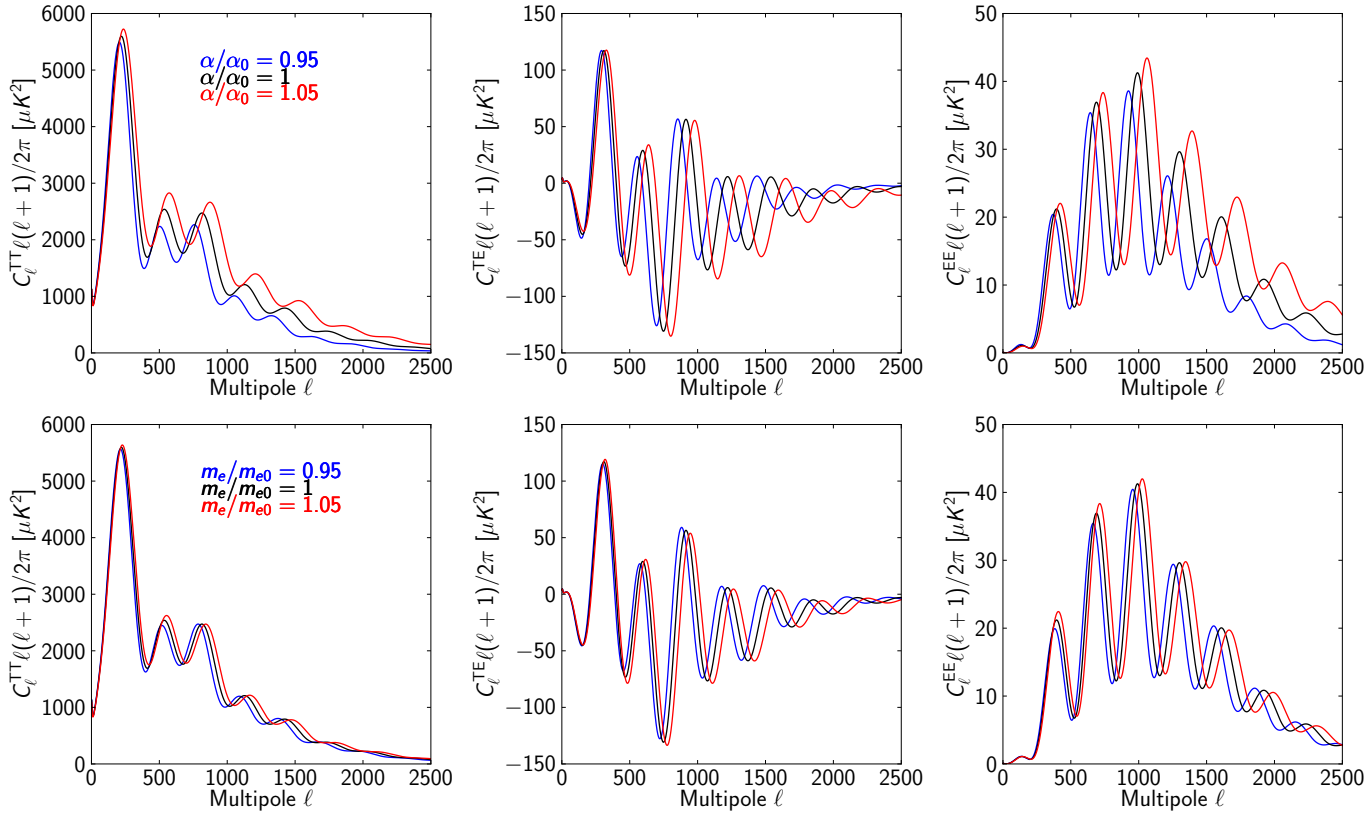

Fig. 2. CMB TT, TE and EE angular power spectra for different values of α (upper plots) and m_e (lower plots). The lines refer to variations of −5% (blue) and +5% (red), while the standard case is shown in black.

with other cosmological parameters, e.g., the *Hubble* constant. However, these degeneracies can be broken, since a change in the value of the constants also affects the amplitude of the peaks, as described below.

The second effect of an earlier recombination is an increase of the amplitude of the peaks at small scales, due to a decrease of the Silk damping (Silk 1968). This effect is, however, more relevant for a change in the fine structure constant rather than for a change in the mass of the electron. This is because the Silk damping length can be defined as (Zaldarriaga & Harari 1995; Hu & Sugiyama 1995; Kaiser 1983)

$$\lambda_{\rm D}^2 = \frac{1}{6}\int_0^{\eta_{\rm dec}} \frac{{\rm d}\eta}{\sigma_{\rm T} n_{\rm e} a}\left[\frac{R^2 + \frac{16}{15}(1+R)}{(1+R)^2}\right], \tag{14}$$

where $R = 3\rho_{\rm b}/(4\rho_{\rm r}) = 3\omega_{\rm b}/(4\omega_\gamma)\,a$, is the baryon-radiation ratio and $\eta_{\rm dec}$ the conformal time of decoupling. An earlier and faster recombination process, due to a larger value of the constants, results in a smaller $\lambda_{\rm D}$ and thus in damping affecting only smaller scales. However, $\lambda_{\rm D}^2$ is also inversely proportional to the Thomson scattering cross-section, which depends on α and $m_{\rm e}$ as (see also Eq. (7))

$$\lambda_{\rm D}^2 \propto \frac{1}{\sigma_{\rm T}} \propto \frac{1}{\alpha^2 m_{\rm e}^{-2}}.$$

Thus, an increase of α decreases the Silk damping scale, not only by precipitating recombination, but also by increasing the Thomson scattering cross-section, as both these effects decrease $\lambda_{\rm D}$. On the other hand, an increase of $m_{\rm e}$ decreases the Thomson scattering cross-section, thus partially compensating for the decrease of $\lambda_{\rm D}$ due to the earlier recombination. For this reason, α has a larger impact on the damping tail than $m_{\rm e}$.

Finally, the third effect of an earlier recombination due to a larger value of the constants is an increase of the amplitude of the spectra at large scales. This is due to the shorter time interval between the redshift of matter-radiation equality and the redshift of decoupling, which has two main consequences. On the one hand, the early integrated Sachs-Wolfe effect (Hu & Sugiyama 1995) is enhanced in the TT power spectrum, increasing the amplitude of the first peak. On the other hand, the baryon-radiation ratio R is smaller at the epoch of recombination. This impacts the amplitude of all the spectra (Hu & Sugiyama 1995), since it decreases the shift of the equilibrium point in the photo-baryonic oscillations due to the baryon load, resulting in a smaller enhancement of the amplitude of odd peaks compared to even ones in the TT power spectrum.

In conclusion, the overall amplitude of the peaks is less affected by a change in $m_{\rm e}$ than by a change in α, due to the different effect on the damping tail. This is the reason why high resolution data on the damping tail, as provided by *Planck*, allow one to break the degeneracy between α and H_0, while one can hardly do this for $m_{\rm e}$ and H_0. Further details of these effects can be found in Appendix B.

2.2. Beyond (α, m_e)

As explained above, only the fine structure constant and the electron mass have a direct impact on the recombination history. This work, as in most previous analyses, assumes that the gravitational sector is not modified, so that the dimensionless Friedmann equation takes its standard form:

$$E^2(z) = \Omega_{\rm m}(1+z)^3 + \Omega_{\rm r}(1+z)^4 + \Omega_K(1+z)^2 + \Omega_\Lambda, \tag{15}$$

with $\Omega_m = \Omega_c + \Omega_b$ and $H(z) = H_0 E(z)$. However, in full generality, and to be self-consistent, the variation of any constant would represent a violation of the Einstein equivalence principle and hence invalidates the use of General Relativity to describe gravitation, and thus cosmology. The Einstein equations, and thus the Friedmann equations, should be modified due to the existence of new degrees of freedom that: (i) couple to the standard matter fields and are responsible for a long range interaction; and (ii) have their own energy densities, which should be included in the Friedmann equation (Ellis & Uzan 2005).

A large number of theoretical extensions to standard physics have been proposed and it is not our purpose here to list and investigate all these ideas. It is, however, useful to mention that we can roughly consider two classes of models. First, one can assume that all masses vary identically, i.e., that m_a/m_b remains constant for all types of field. Such a theory can be rewritten as a varying G theory, i.e., as a scalar-tensor theory (Will 1981). Cosmological signatures of these theories have been discussed in, e.g., Damour & Pichon (1999) and Coc et al. (2006) for big-bang nucleosynthesis (BBN); a complete and consistent description of their signatures on the CMB can be found in Riazuelo & Uzan (2002), to be compared to the phenomenological approaches adopted in Zahn & Zaldarriaga (2003) and Galli et al. (2009). It is however important to realize that as soon as one assumes that α is varying, one expects the masses of all nucleons to vary as well, since the field responsible for the variation of α couples radiatively to nucleons. We thus expect the proton and neutron masses to be time dependent (Olive & Pospelov 2002), even if one assumes that the masses of all fundamental particles remain constant, in which case the model cannot be rephrased as a varying G theory.

Another aspect of the variation fundamental constants, which has been much discussed in the literature (see e.g., Dicke 1962; Duff 2002; Uzan 2003; Narimani et al. 2012), is that only dimensionless combinations of constants can really be measured. Because of this, many previous studies have focussed on the parameter $\mu \equiv m_e/m_p$. We have checked that for the physics of recombination our consideration of m_e is entirely equivalent to variation of μ. Hence our study of constraints on (α, m_e) is consistent with arguments that the only meaningful variations are dimensionless ones. However, the situation would be more complicated if we were to consider additional constants, and in particular G. As already stated, G enters the Friedmann equation, and so even if one considers a dimensionless ratio, such as $Gm_p^2/\hbar c$, there are still complications over whether the cosmological framework is even self-consistent, in addition to whether the cosmological perturbations might evolve differently. This can only be done within the context of specified theories of modified gravity.

This short discussion emphasizes the difficulty in implementing in a self-consistent way the variation of several constants without fully specifying a theory, thus becoming model-dependent. Let us also point out that in many specific constructions the variations of the different constants are correlated (see, e.g., Coc et al. 2007; Luo et al. 2011) and will enter both the equations governing the dynamics of the background spacetime, i.e., new terms in Eq. (15), and the recombination process. In our work, we focus on the two constants that have a dominant effect on the recombination history, and we have neglected their effect on the background expansion, which is a good approximation for small variations. However, it is important to keep in mind that this is an approximation, and that one should in principle rely on a completely defined theoretical model (see, e.g., Damour & Pichon 1999; and Coc et al. 2006 for cases in which such an approximation is not accurate).

3. Time variation of a single constant

3.1. Standard Planck data analysis

In this section we determine the *Planck* constraints on the value of the fine-structure constant α and on the mass of the electron m_e, assuming that only one constant can vary at a time.

The cosmological picture we assume is a flat ΛCDM model with one additional varying constant (α or m_e), purely adiabatic initial conditions with an almost scale invariant power spectrum, and no primordial gravity waves. It is thus described by a seven-dimensional parameter space that includes the baryon and cold dark matter densities $\omega_b = \Omega_b h^2$ and $\omega_c = \Omega_c h^2$, the Hubble constant H_0, the optical depth at reionization τ, the scalar spectral index n_s, the overall normalization of the spectrum A_s (defined here at $k = 0.05$ Mpc^{-1}) and a parameter for the varying constant:

$$\{\omega_b, \omega_c, H_0, \tau, n_s, A_s, \alpha \text{ or } m_e\}.$$

Unless otherwise stated, we derive the value of the primordial helium abundance as in Hamann et al. (2011). This uses interpolated results from the `PArthENoPE` BBN code (Pisanti et al. 2008), which calculates the value of the helium abundance given the number of relativistic species N_{eff} and the physical baryon density ω_b, assuming standard BBN. Furthermore, unless explicitly varied, we fix the number of relativistic species to $N_{eff} = 3.046$ and the sum of the neutrino masses to $\sum m_\nu = 0.06$ eV, as in Planck Collaboration XVI (2014).

In order to determine the constraints, we use *Planck* temperature anisotropy data (Planck Collaboration XV 2014) in combination with several other data sets, and use the likelihood code publicly released by the *Planck* collaboration[4]. We use the same assumptions and data sets used in Planck Collaboration XVI (2014) to determine the cosmological parameters, and we refer the reader to this paper for further details. The data sets we use are:

- *Planck*. The *Planck* CMB power spectra are analysed using two different likelihood codes. In the multipole range $2 \leq \ell \leq 49$, the likelihood is based on a component-separation approach over 91% of the sky (Planck Collaboration XII 2014; Planck Collaboration XV 2014), while at higher multipoles it is constructed from cross-spectra over the frequency range 100−217 GHz, as discussed in Planck Collaboration XV (2014). In the latter case, the amplitude of unresolved foregrounds, as well as beam and calibration uncertainties, are explored, along with the cosmological parameters. In the following, we will refer to the combination of these two likelihoods simply as *Planck*.
- *WP*. In combination with the *Planck* temperature data, we include polarization data from the WMAP satellite (Bennett et al. 2013) in the multipole range $2 < \ell < 23$, using the likelihood code provided by the *Planck* collaboration. We will refer to this data set as WP.
- *Lensing*. We include information from the lensing potential power spectrum $C_\ell^{\phi\phi}$, as determined from the trispectrum computed on *Planck*'s maps. We specifically use the data and likelihood provided in Planck Collaboration XVII (2014).

[4] http://pla.esac.esa.int/pla/aio/planckProducts.html

Table 2. Constraints on cosmological parameters for a ΛCDM model with the addition of a varying fine-structure constant.

Parameter	*Planck*+WP 68% limits	*Planck*+WP+highL 68% limits	*Planck*+WP+BAO 68% limits	*Planck*+WP+HST 68% limits	*Planck*+WP+lensing 68% limits	WMAP-9 68% limits
$\Omega_b h^2$	0.02207 ± 0.00028	0.02212 ± 0.00028	0.02220 ± 0.00026	0.02226 ± 0.00028	0.02218 ± 0.00027	0.0231 ± 0.0013
$\Omega_c h^2$	0.1173 ± 0.0031	0.1183 ± 0.0030	0.1160 ± 0.0029	0.1167 ± 0.0031	0.1162 ± 0.0027	0.1145 ± 0.0048
H_0	$65.1^{+1.7}_{-1.9}$	66.2 ± 1.7	66.8 ± 1.2	68.3 ± 1.5	65.9 ± 1.7	74^{+10}_{-10}
τ	$0.095^{+0.013}_{-0.016}$	$0.095^{+0.013}_{-0.016}$	$0.097^{+0.014}_{-0.016}$	$0.095^{+0.013}_{-0.016}$	$0.095^{+0.013}_{-0.015}$	$0.089^{+0.013}_{-0.015}$
α/α_0	0.9934 ± 0.0042	0.9964 ± 0.0037	0.9955 ± 0.0039	0.9991 ± 0.0039	0.9938 ± 0.0043	1.007 ± 0.020
n_s	0.975 ± 0.012	0.967 ± 0.011	0.975 ± 0.012	0.969 ± 0.012	0.977 ± 0.011	0.974 ± 0.014
$\ln(10^{10} A_s)$ . . .	$3.106^{+0.027}_{-0.033}$	$3.101^{+0.026}_{-0.031}$	$3.104^{+0.028}_{-0.033}$	$3.095^{+0.027}_{-0.031}$	$3.102^{+0.026}_{-0.029}$	3.090 ± 0.038

Notes. We quote errors at the 68% confidence level. The Hubble constant H_0 is in units of km s^{-1} Mpc^{-1}.

- *highL* We combine *Planck* data with CMB TT information coming from ground-based high resolution experiments. We use the 2013 data release of the Atacama Cosmology Telescope (ACT) as described in Das et al. (2014), in particular, the ACT 148 × 148 GHz power spectrum at $\ell > 1000$, and the ACT 148×218 GHz and 218×218 GHz power spectra at $\ell > 1500$. Furthermore, we use the 2012 data release of the South Pole Telescope (SPT), as described in Reichardt et al. (2012), including data at $\ell > 2000$.
- *BAO* We also present results using Baryon Acoustic Oscillation (BAO) data from the following redshift surveys: the SDSS DR7 measurement at $z = 0.35$ (Padmanabhan et al. 2012); the BOSS DR9 measurement at $z = 0.57$ (Anderson et al. 2013); and the 6dF Galaxy Survey measurement at $z = 0.1$ (Beutler et al. 2011).
- HST We include a Gaussian prior on the Hubble constant H_0 as determined by Riess et al. (2011),

$$H_0 = (73.8 \pm 2.4) \text{ km s}^{-1} \text{ Mpc}^{-1}, \quad (16)$$

using cepheids and type Ia supernovae (SNe Ia). This value is determined using *Hubble* Space Telescope (HST) observations of cepheid variables in the host galaxies of eight type Ia SNe to calibrate the supernova magnitude-redshift relation.

In the following, we also present results using the WMAP-9 data release (temperature and polarization), utilizing the likelihood code provided by the WMAP team (Bennett et al. 2013).

We use a modified version of the `RECFAST` (v. 1.5.2)[5] recombination code (Seager et al. 1999; Hannestad 1999; Martins et al. 2004b; Rocha et al. 2004; Menegoni et al. 2009) to include the variation of constants, as described in Sect. 2.1. To calculate constraints, we use the publicly available Markov Chain Monte Carlo (MCMC) package `cosmomc` (Lewis & Bridle 2002). The MCMC convergence diagnostic tests are performed on four chains using the Gelman and Rubin "variance of chain mean"/"mean of chain variances" $R - 1$ statistic for each parameter (Gelman & Rubin 1992). Our constraints are obtained after marginalization over the remaining "nuisance" parameters, again using the programs included in the `cosmomc` package. We use a cosmic age top-hat prior of $10\,\text{Gyr} \leq t_0 \leq 20\,\text{Gyr}$, which is wide enough to have no affect on our results. We sample the seven-dimensional set of cosmological parameters, adopting flat priors on them, together with foreground, beam and calibration parameters when using the *Planck* data (14 additional parameters) and the highL data (17 additional parameters). For these "non-cosmological" parameters we use the same assumptions and priors as in table 4 of Planck Collaboration XVI (2014).

[5] Available at `http://www.astro.ubc.ca/people/scott/recfast.html`.

Table 3. Constraints on cosmological parameters for a ΛCDM model.

Parameter	*Planck*+WP 68% limits
$\Omega_b h^2$	0.02204 ± 0.00029
$\Omega_c h^2$	0.1199 ± 0.0027
H_0	67.3 ± 1.2
τ	$0.089^{+0.012}_{-0.014}$
n_s	0.9606 ± 0.0075
$\ln(10^{10} A_s)$	3.089 ± 0.024

Notes. We quote errors at the 68% confidence level. The Hubble constant H_0 is in units of km s^{-1} Mpc^{-1}.

3.2. Fine structure constant (α)

The results of the analysis on the variation of the fine structure constant are summarized in Table 2, which compares parameter constraints from *Planck* (combined with different data sets) and those obtained with WMAP-9 data. As a comparison, we also show the constraints from *Planck* for a standard ΛCDM model in Table 3. Figure 3 compares the one-dimensional likelihood profiles for α obtained with different data sets, while Fig. 4 shows the degeneracies between α and the six other cosmological parameters used in our analysis.

From CMB data alone, *Planck* improves the constraints from a 2% variation on α (from WMAP-9) to about 0.4% (in agreement with what was found in Table 11 of Planck Collaboration XVI 2014). *Planck* thus improves the limit by about a factor of five, in good agreement from what was expected from previous forecasts (see e.g., Rocha et al. 2004; Galli et al. 2010). The improvement is mainly due to the fact that *Planck* is able to break the strong degeneracy between α and H_0 by observing the damping tail, as already pointed out in Sect. 2.1. This constraint is also better (although of comparable

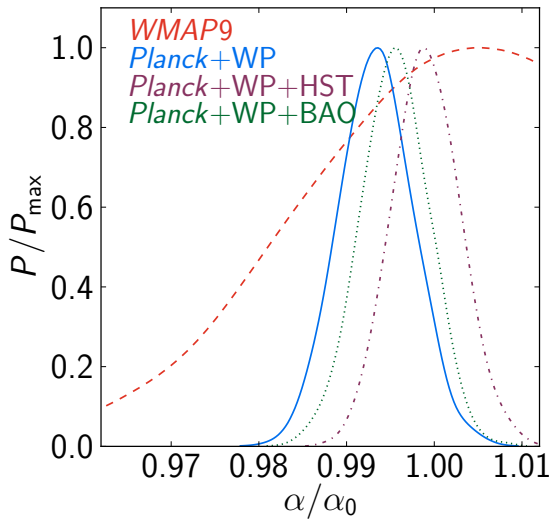

Fig. 3. Marginalized posterior distributions of α/α_0 obtained using WMAP-9 (red dashed), *Planck*+WP (blue solid), *Planck*+WP+HST (purple dot-dashed) and *Planck*+WP+BAO (green dotted) data combinations.

magnitude) than the one obtained by combining WMAP data with small-scale experiments (see, e.g., Sievers et al. 2013, for a 0.5% constraint).

We also observe that the constraints on the parameters of the reference ΛCDM model change very little with the addition of a varying α, exceptions being for n_s and H_0. In fact, the constraint on n_s for *Planck*+WP is 0.9603 ± 0.0073 assuming a ΛCDM model, while it is 0.974 ± 0.012 for a ΛCDM+α model; the mean value of n_s shifts about 1σ to higher values and the uncertainty increases by a factor of 1.6. On the other hand, the constraint on H_0 in a ΛCDM model is (67.3 ± 1.2) km s^{-1} Mpc^{-1}, while in a ΛCDM+α model it is (65.1 ± 1.8) km s^{-1} Mpc^{-1}. Thus, the value of the Hubble constant shifts by about 1.2σ to even lower values; this exacerbates the tension with the value of the Hubble constant found by Riess et al. (2011) and reported in Eq. (16).

Finally, we find that α is weakly degenerate with foreground, beam and calibration parameters, as shown in Fig. C.1.

3.2.1. The low- versus high-ℓ tension and α

The value of α/α_0 found using *Planck*+WP data and reported in Table 2 is 1.6σ lower than unity. Although this is statistically not very significant, it is interesting to emphasize that this deviation is mainly caused by the apparent "tension" between the low and high multipoles in the *Planck* data; as already found in Planck Collaboration XV (2014) and Planck Collaboration XVI (2014), this tension is partially responsible for small hints of anomalies found by the *Planck* collaboration when exploring extensions of the ΛCDM model. In order to assess the importance of this effect for the fine structure constant, we remove the *Planck* low-ℓ likelihood in temperature and the WMAP low-ℓ likelihood in polarization, and add a Gaussian prior to constrain the reionization optical depth, $\tau = 0.09 \pm 0.013$; this value approximates the constraint obtained by Hinshaw et al. (2013) using WMAP polarization data. The results of this exercise are shown in Table C.3. As expected, for the *Planck*(−low ℓ)+τ prior case, the constraint for α/α_0 is 0.9972 ± 0.0052, in agreement with unity within 1σ.

3.2.2. Combination with other data sets

We can combine *Planck* data with a number of different data sets, as already described in Sect. 3.1. We find that adding highL data improves the constraint on α by a small amount, as most of the meaningful information on the damping tail is already provided by *Planck*. Similarly, adding BAO data does not improve the error bars significantly.

Given the apparent tension between the reference ΛCDM parameters from *Planck* and direct measurements of H_0 (see e.g., Planck Collaboration XVI 2014), we also investigate the effect of including HST data, although the value of the Gaussian prior on H_0 in Eq. (16) is roughly 4σ higher than the value of H_0 obtained with the *Planck*+WP data in Table 2. Adding the prior on H_0 has the effect of increasing the mean value of α to be closer to α_0, due to the positive correlation between the two parameters. However, the uncertainty on α/α_0 does not improve significantly.

3.3. Fine structure constant, number of relativistic species and helium abundance

In order to assess the robustness of our constraints to the chosen cosmological model, we explore how much the constraint on α is weakened when the number of relativistic species ($N_{\rm eff}$) or the helium abundance (Y_p) are allowed to vary as well. We thus explore in this case an eight-dimensional parameter space that includes the six ΛCDM parameters, together with α and $N_{\rm eff}$ or Y_p. A degeneracy between these parameters can be expected (see e.g., Menegoni et al. 2012) since they change the position and the amplitude of the peaks in similar ways (see e.g., Hou et al. 2013; Hinshaw et al. 2013). In fact, $N_{\rm eff}$ changes the angular scale of Silk damping with respect to the angular scale of the peaks, while varying Y_p changes the recombination history, and in particular the recombination time and the Thomson scattering rate before recombination. Since these effects could also come about through a change in the fine structure constant, we could expect degeneracies between these parameters. Table C.1 shows the constraints on parameters for the ΛCDM+α+$N_{\rm eff}$ model, while Fig. 5 shows the important degeneracy present between α and $N_{\rm eff}$. We find that including a variable number of relativistic species increases the uncertainties on the value of α, from $\alpha/\alpha_0 = 0.9934 \pm 0.0042$ to $\alpha/\alpha_0 = 0.9933^{+0.0071}_{-0.0045}$ when $N_{\rm eff}$ is also allowed to vary. Furthermore, we find that the constraint on the number of relativistic species in this case, $N_{\rm eff} = 3.04^{+0.54}_{-0.73}$, remains in perfect agreement with the standard value $N_{\rm eff} = 3.046$.

On the other hand, we observe a much stronger degeneracy between α and Y_p, as shown in Table C.2 and Fig. 6. We find that leaving the helium abundance completely free to vary in the range $0.08 < Y_p < 0.55$ leads to a constraint on α at the 1% level, while the value of Y_p is almost unconstrained[6]. We emphasize that the chosen variation range for Y_p is unphysically large, considering the latest spectroscopic constraints on primordial helium abundance yield $Y_p = 0.2465 \pm 0.0097$ (Aver et al. 2013).

3.4. Mass of the electron (m_e)

Now we present the results of our analysis on the variation of the electron mass, adopting the same procedure followed

[6] We checked that the flat prior we impose on the age of the Universe, described in Sect. 3.1, does not affect these constraints.

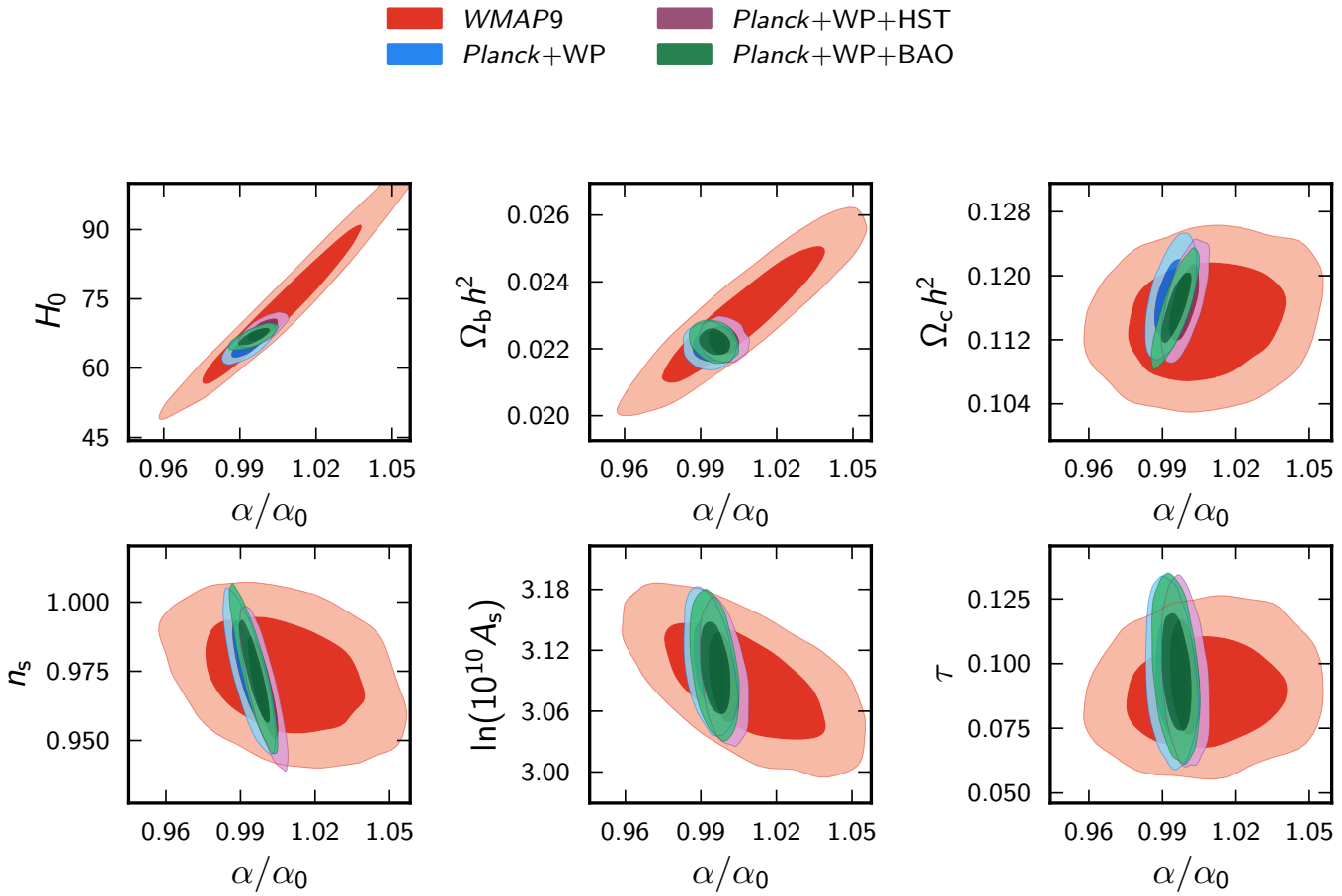

Fig. 4. Two-dimensional likelihood contours (68% and 95%) for α/α_0, versus other cosmological parameters for the WMAP-9 (red), *Planck*+WP (blue), *Planck*+WP+HST (purple), and *Planck*+WP+BAO (green) data combinations.

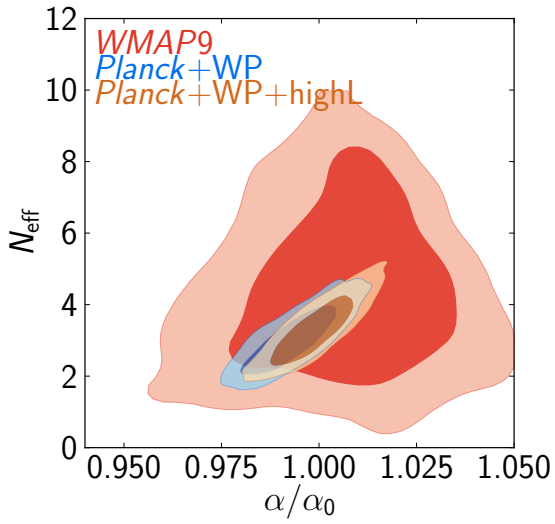

Fig. 5. Two-dimensional likelihood contours (68% and 95%) in the $(\alpha/\alpha_0, N_{\rm eff})$ plane for WMAP (red), *Planck*+WP (blue), and *Planck*+WP+highL (orange) data combinations.

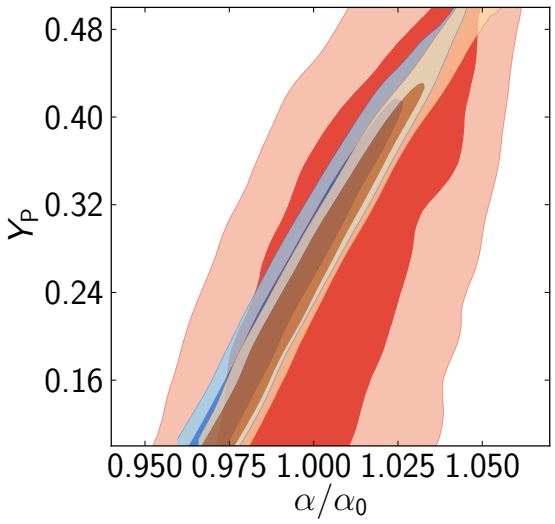

Fig. 6. Two-dimensional likelihood contours (68% and 95%) in the $(\alpha/\alpha_0, Y_p)$ plane for WMAP (red), *Planck*+WP (blue) and *Planck*+WP+highL (orange) data combinations.

for the variation of α that was described in the previous sections. Here we assume the fine structure constant to be fixed to its standard value and consider variations of $m_{\rm e}$. The results of the analysis are presented in Table 4, while Fig. 7 depicts the one-dimensional likelihood profiles for $m_{\rm e}$ determined with different combinations of data. Fig. 8 shows the two-dimensional contour plots between $m_{\rm e}$ and the other cosmological parameters. The constraint obtained from *Planck*+WP is $m_{\rm e}/m_{\rm e0} = 0.977^{+0.055}_{-0.070}$, 68% CL, to be compared to the one obtained with WMAP-9 data, $m_{\rm e}/m_{\rm e0} = 1.011^{+0.077}_{-0.057}$. It is

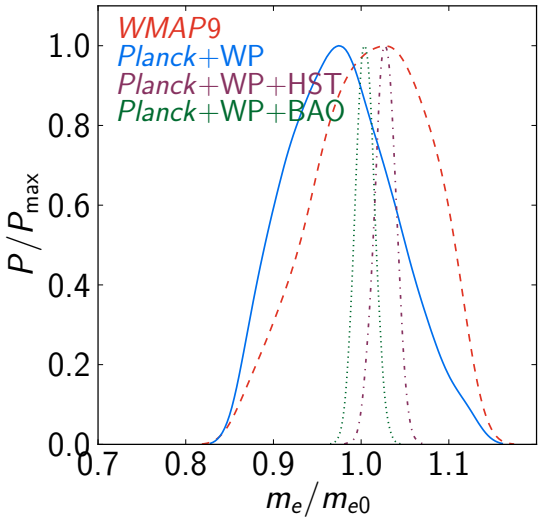

Fig. 7. Marginalized posterior distributions of m_e/m_{e0} obtained using WMAP-9 (red dashed), *Planck*+WP (blue solid), *Planck*+WP+HST (purple dot-dashed) and *Planck*+WP+BAO (green dotted) data combinations.

interesting to note that in the case of m_e, *Planck* is not able to efficiently break the degeneracy with the Hubble constant, contrary to what happens for the fine structure constant. This is due to the fact that m_e does not strongly change the amplitude of the damping tail, as detailed in Sect. 2.1 and Appendix B.

We also find that, similarly to the case of the fine structure constant, m_e is not strongly correlated with foreground, beam and calibration parameters. This is shown in Fig. C.2. In Table C.4 we also show the effect of removing the low-ℓ multipoles and placing a Gaussian prior on the optical depth. We find that for the electron mass (just as we found for α), the effect of suppressing the low multipoles is to increase the mean value of m_e/m_{e0} to values closer to unity, by typically 0.5σ.

Unlike the case of the fine structure constant, the constraint on m_e/m_{e0} is not dramatically improved by *Planck* data compared to the WMAP constraint, due to the strong degeneracy with H_0. However, we find that adding external data sets can dramatically break this degeneracy. As shown in Table 4, including BAO data decreases the uncertainty on m_e/m_{e0} by a factor of around 5, from $m_e/m_{e0} = 0.977^{+0.055}_{-0.070}$ to $m_e/m_{e0} = 1.004 \pm 0.011$.

Similarly, adding HST data provides a tight constraint at roughly the 1% level, $m_e/m_{e0} = 1.027 \pm 0.012$; however, in this case, the mean value of m_e/m_{e0} is 2.3σ higher than unity. This is expected from the positive correlation between m_e/m_{e0} and H_0 and from the "high" (compared to the *Planck* determination) HST value of H_0.

4. Simultaneous variation of α and m_e

The previous analysis can easily be generalized to include simultaneous variations of the electron mass m_e and α. We follow exactly the same procedure as in the previous section but now with an 8-dimensional parameter space. The constraint in the plane (α, m_e) is depicted in Fig. 9, while constraints on single parameters are presented in Table 5. It is interesting to note that the constraints on α are not substantially changed by varying m_e at the same time, as we obtain $\alpha/\alpha_0 = 0.993 \pm 0.0045$ and $m_e/m_{e0} = 0.994 \pm 0.059$. This is due to the fact that the effect of the fine structure constant on the damping tail is different enough to break the degeneracy both with m_e and H_0, as described in Appendix B.

5. Spatial variation of α

Recent analyses of quasar absorption spectra data have led to a claim that there might exist a dipole in the fine structure constant (Webb et al. 2011; Berengut et al. 2011; King et al. 2012). Combining the observations of 154 absorption systems from VLT and 161 absorption systems from the Keck telescope, it was concluded (King et al. 2012) that the variation of the fine structure constant is well-represented by an angular dipole pointing in the direction RA $= 17.3\ h \pm 1.0\ h$, Dec $= -61^\circ \pm 10^\circ$, with amplitude $\Delta\alpha/\alpha = 0.97^{+0.22}_{-0.20} \times 10^{-5}$ (68% CL). This measured value thus appears to be discrepant with zero at the 4σ level. However, this claim has been met with some scepticism. Webb et al. themselves admitted the presence of an unexplained error term in the quasar data set, and a compilation of potential issues in their analysis can be found in Cameron & Pettitt (2012) and Cameron & Pettitt (2013). In these studies, it is argued that the close alignment between the equator of the dipole and the North-South divide between the typical sight lines of the two telescopes (VLT and Keck) used to collect the data might play a role in the detection of a dipole modulation; systematic errors of opposite signs could be responsible for the apparent signal. Furthermore, all estimates of statistical significance in Webb et al. (2011) assumed unbiased Gaussian errors, but this might not be correct in the case considered. Finally Cameron & Pettitt (2012) performed a parametric Bayesian model selection analysis of the very same data set as Webb et al. (2011), pointing out an incomplete understanding of the observational errors and a lack of theoretical expectation for a spatial variation of α. All these issues motivate us to test for dipole modulation of α using different methods and alternative kinds of data.

From a theoretical point of view, a dipolar modulation could be realized in some models (Olive et al. 2011, 2012) and extend to high redshift. Moreover, it was pointed out that a specific signature on the CMB anisotropy is expected (Moss et al. 2011) if we simply consider a gradient in α across our Hubble volume. Such a modulation is different from a randomly fluctuating fine structure constant, which may appear if α depends on a light scalar field that has developed super-Hubble correlations during inflation. A spatial fluctuation of the fine structure constant also induces non-Gaussian temperature and polarization correlations in the CMB, as well as B-modes in the polarization (Sigurdson et al. 2003; Pitrou et al. 2008). The amplitude of such a stochastic fluctuation has recently been constrained to be $\delta\alpha/\alpha_0 = (1.34 \pm 5.82) \times 10^{-2}$ at the 95% confidence level (O'Bryan et al. 2013) on scales larger than 10° using *Planck* data.

Here we will search specifically for a dipole signature on the last-scattering surface. We first recall in Sect. 5.1 the effect of a spatial variation of fundamental constants on the CMB, in order to show that it implies mode couplings between the $a_{\ell m}$. We describe a statistical estimator based on Hanson & Lewis (2009) in Sect. 5.2. This estimator is then used in *Planck*-like simulations without (Sect. 5.3) and with (Sect. 5.4) a dipole modulation in α in order to study the effect of the masking, which induces additional bias in this estimator. We calibrate the estimator in Sect. 5.5, and we finally apply the method to the *Planck* data in Sect. 5.6.

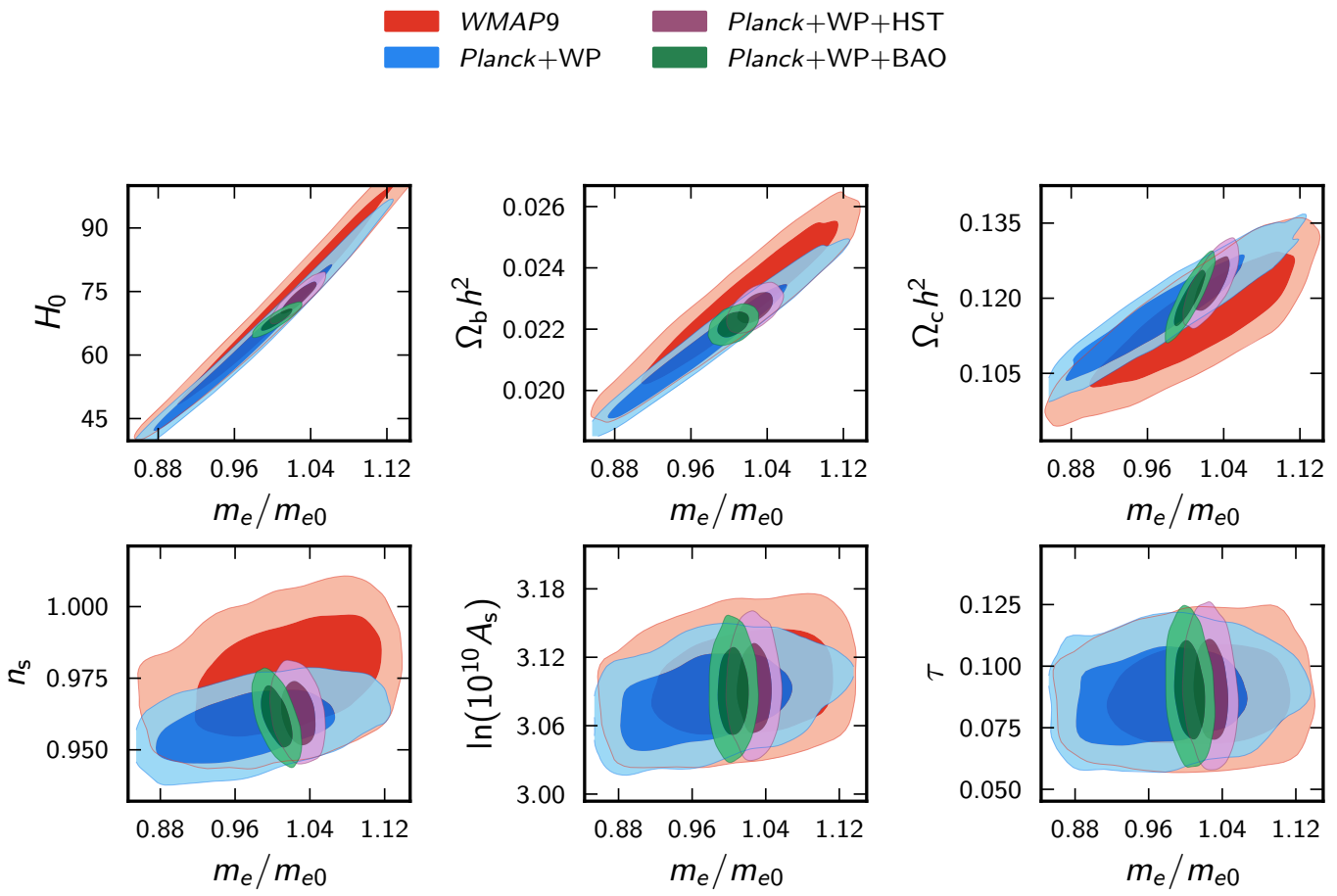

Fig. 8. Two-dimensional likelihood contours (68% and 95%) for m_e/m_{e0} versus other cosmological parameters, for the WMAP-9 (red), *Planck*+WP (blue), *Planck*+WP+HST (purple), and *Planck*+WP+BAO (green) data combinations.

Table 4. Constraints on the cosmological parameters of the base ΛCDM model with the addition of a varying electron mass.

Parameter	*Planck*+WP 68% limits	*Planck*+WP+highL 68% limits	*Planck*+WP+BAO 68% limits	*Planck*+WP+HST 68% limits	*Planck*+WP+lensing 68% limits	WMAP-9 68% limits
$\Omega_b h^2$	$0.0215^{+0.0013}_{-0.0016}$	$0.0215^{+0.0012}_{-0.0015}$	0.02216 ± 0.00027	0.02270 ± 0.00033	$0.0215^{+0.0013}_{-0.0014}$	$0.0229^{+0.0019}_{-0.0015}$
$\Omega_c h^2$	$0.1172^{+0.0070}_{-0.0087}$	$0.1171^{+0.0067}_{-0.0080}$	0.1201 ± 0.0036	0.1229 ± 0.0035	$0.1147^{+0.0069}_{-0.0078}$	0.1154 ± 0.0083
H_0	63^{+10}_{-20}	63^{+10}_{-10}	68.4 ± 1.7	73.5 ± 2.4	62^{+10}_{-10}	72 ± 10
τ	$0.088^{+0.012}_{-0.014}$	$0.090^{+0.012}_{-0.014}$	$0.091^{+0.012}_{-0.014}$	$0.091^{+0.013}_{-0.014}$	$0.088^{+0.012}_{-0.014}$	$0.089^{+0.013}_{-0.015}$
m_e/m_{e0}	$0.977^{+0.055}_{-0.070}$	$0.976^{+0.053}_{-0.064}$	1.004 ± 0.011	1.027 ± 0.012	0.969 ± 0.055	$1.011^{+0.077}_{-0.057}$
n_s	0.9584 ± 0.0083	0.9565 ± 0.0077	0.9614 ± 0.0068	0.9628 ± 0.0072	0.9618 ± 0.0070	0.975 ± 0.014
$\ln(10^{10}A_s)$ . . .	3.084 ± 0.027	$3.085^{+0.024}_{-0.026}$	3.091 ± 0.025	$3.093^{+0.024}_{-0.027}$	3.079 ± 0.025	3.097 ± 0.032

Notes. We quote $\pm 1\sigma$ errors here. We note that for WMAP there is a strong degeneracy between H_0 and m_e, which is why the uncertainty on m_e/m_{e0} is much larger than for *Planck*.

5.1. Dipolar modulation in the fundamental constants

Following the claim of Webb et al. (2011), we assume that some constants c_p have a spatial variation that can be described by a dipolar modulation, i.e.,

$$c_p(\hat{\boldsymbol{n}}, z) = c_p(z) + \sum_{i=-1}^{1} \delta c_p^{(i)}(z) Y_{1i}(\hat{\boldsymbol{n}}). \quad (17)$$

Here the monopole $c_p(z) = c_{p,0}$ is assumed to be independent of time (otherwise we are back to the analysis of the previous sections), so that it reduces to the value measured locally today. The quantities $\delta c_p^{(i)}$ are three parameters that characterize the amplitude and direction of the modulation, the amplitude δc_p being defined as

$$\delta c_p \equiv \frac{1}{2}\sqrt{\frac{3}{\pi}}\sqrt{|\delta c_p^{(0)}|^2 + 2|\delta c_p^{(1)}|^2}. \quad (18)$$

Table 5. Constraints on the cosmological parameters for the base ΛCDM model with the simultaneous addition of a varying fine-structure constant and mass of the electron.

Parameter	*Planck*+WP 68% limits	*Planck*+WP+highL 68% limits	WMAP-9 68% limits
$\Omega_b h^2$	0.0219 ± 0.0014	$0.0216^{+0.0013}_{-0.0016}$	$0.0230^{+0.0018}_{-0.0015}$
$\Omega_c h^2$	0.1166 ± 0.0069	$0.1156^{+0.0069}_{-0.0081}$	0.115 ± 0.010
H_0	64^{+10}_{-10}	62^{+10}_{-20}	73 ± 10
τ	$0.095^{+0.014}_{-0.016}$	$0.093^{+0.013}_{-0.016}$	$0.090^{+0.014}_{-0.015}$
α/α_0	0.9933 ± 0.0045	0.9963 ± 0.0037	$1.006^{+0.025}_{-0.034}$
m_e/m_{e0}	0.994 ± 0.059	$0.976^{+0.057}_{-0.066}$	1.004 ± 0.091
n_s	0.974 ± 0.014	0.965 ± 0.012	0.975 ± 0.018
$\ln(10^{10} A_s)$	$3.105^{+0.030}_{-0.034}$	3.096 ± 0.030	3.093 ± 0.051

Notes. We quote 68% CL uncertainties.

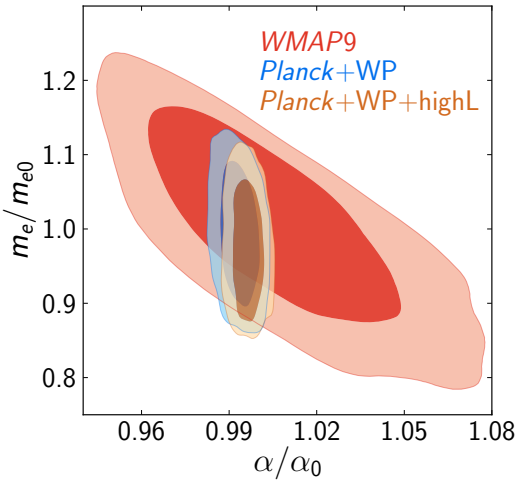

Fig. 9. Two-dimensional likelihood contours (68% and 95%) in the $(\alpha/\alpha_0, m_e/m_{e0})$ plane for *Planck*+WP (blue) and *Planck*+WP+highL (yellow) data combinations. We also show the results using WMAP data in red.

Since $c_p(\hat{\boldsymbol{n}}, z)$ has to be real, they are related by

$$\delta c_p^{(0)} \in \mathbb{R}, \qquad \delta c_p^{(+1)} = -\left[\delta c_p^{(-1)}\right]^*. \tag{19}$$

As a consequence studying $\{\delta c_p^{(0)}, \delta c_p^{(1)}, \delta c_p^{(-1)}\}$ is equivalent to studying $\{\delta c_p^{(0)}, \mathrm{Re}(\delta c_p^{(1)}), \mathrm{Im}(\delta c_p^{(1)})\}$. For simplicity, we assume that $\delta c_p^{(i)}$ does not depend on redshift in the range probed by primary CMB anisotropies (i.e., $600 < z <$ few $\times 10^6$). This is a good approximation as long as: (i) we do not include the variation of the gravitational constant or other physics in the early Universe; and (ii) there is no high frequency variation compared to the time scale fixed by the Hubble time at recombination (see Footnote 3). This means effectively that we are assuming there is a well-defined value of α in every direction on the last-scattering surface, but that the value could depend on direction, with a $\cos\theta$ dependence. The monopole is the value of the constant at last-scattering – which for the purposes of this section we assume to be the same as the value today.

As previously explained, any change in the constants induces a change in the dynamics of the recombination process. It follows that the CMB temperature anisotropy will be modulated as

$$\Theta(\hat{\boldsymbol{n}}) = \Theta[\hat{\boldsymbol{n}}, c_p(\hat{\boldsymbol{n}})] \tag{20}$$

$$= \Theta\left[\hat{\boldsymbol{n}}, c_{p,0} + \sum_{i=-1}^{1} \delta c_p^{(i)} Y_{1i}(\hat{\boldsymbol{n}})\right]$$

$$\simeq \bar{\Theta}(\hat{\boldsymbol{n}}) + \sum_p \sum_{i=-1}^{+1} \frac{\partial \bar{\Theta}(\hat{\boldsymbol{n}})}{\partial c_p} \delta c_p^{(i)} Y_{1i}(\hat{\boldsymbol{n}}), \tag{21}$$

where, again, $\bar{\Theta}$ refers to the usual temperature fluctuation field, which is computed assuming the standard values of the constants and which is statistically homogeneous and isotropic. In the following, we assume that Θ depends only on c_p, but not on its space-time derivative. On the one hand, this is a good approximation when dealing with a dipole fluctuation of weak amplitude because higher orders will be negligible. However, at a theoretical level the dependence of $\bar{\Theta}$ versus $\hat{\boldsymbol{n}}$ might be more complicated, depending on the model.

Decomposing both $\Theta(\hat{\boldsymbol{n}})$ and $\bar{\Theta}(\hat{\boldsymbol{n}})$ in spherical harmonics, as in Eq. (1), it can be shown that (see Prunet et al. 2005, for details):

$$a_{\ell m} = \bar{a}_{\ell m} + \sqrt{\frac{3}{4\pi}} \sum_p \sum_i \delta c_p^{(i)} (-1)^m \sum_{LM} \frac{\partial \bar{a}_{LM}}{\partial c_p} \tag{22}$$

$$\times \sqrt{(2\ell+1)(2L+1)} \begin{pmatrix} \ell & L & 1 \\ -m & M & i \end{pmatrix} \begin{pmatrix} \ell & L & 1 \\ 0 & 0 & 0 \end{pmatrix}.$$

Because of the triangular inequality, the Wigner 3j-symbols are non-zero only when $L = \ell \pm 1$ and $M = m - i$, so that $a_{\ell m}$ is in fact a sum involving $\bar{a}_{\ell m}$ and $\bar{a}_{\ell \pm 1\ m-i}$.

It is clear from Eq. (22) that such a dipolar modulation will develop $(\ell, \ell+1)$ correlations that can be characterized by the two quantities

$$D_{\ell m}^{(i)} \equiv \left\langle a_{\ell m}\, a_{\ell+1\ m+i}^* \right\rangle \tag{23}$$

for $i = 0, 1$. The $D_{\ell m}$s will be non-zero only if any of the $\delta c_p^{(i)}$ are non-zero. Using the usual diagonal covariance property of the $\bar{a}_{\ell m}$, we deduce that

$$D_{\ell m}^{(i)} = f_i(\ell, m) \sum_p \delta c_p^{(i)} \Gamma_\ell^{(p)}, \tag{24}$$

with

$$f_0(\ell,m) = \sqrt{\frac{3}{4\pi}}\frac{\sqrt{(\ell+1)^2-m^2}}{\sqrt{(2\ell+1)(2\ell+3)}}, \quad (25)$$

$$f_1(\ell,m) = \sqrt{\frac{3}{8\pi}}\sqrt{\frac{(\ell+2+m)(\ell+1+m)}{(2\ell+1)(2\ell+3)}}, \quad (26)$$

and where we have defined the quantity

$$\Gamma_\ell^{(p)} \equiv \frac{1}{2}\left(\frac{\partial\bar{C}_\ell}{\partial c_p}+\frac{\partial\bar{C}_{\ell+1}}{\partial c_p}\right). \quad (27)$$

A central ingredient here is the quantity $\partial\bar{C}_\ell/\partial c_p$, the computation of which is detailed in Appendix A and explicitly given in Fig. A.1 for the case $c_p = \alpha$. We would like to point out that essentially the same estimator for dipole modulation, introduced by Prunet et al. (2005), has been used to discuss power asymmetry Hanson & Lewis (2009), aberration (e.g., Planck Collaboration XXVII 2014), and more general parameter anisotropy (Moss et al. 2011), through substituting different c_p.

This construction assumes that we are using the full sky, and one needs to keep in mind that any mask will violate isotropy and induce additional correlations, and thus bias any estimator. In general the temperature field on a masked sky is given by

$$\Theta(\hat{\boldsymbol{n}}) = \left\{\bar{\Theta}(\hat{\boldsymbol{n}}) + \sum_p \sum_{i=-1}^{+1} \frac{\partial\bar{\Theta}(\hat{\boldsymbol{n}})}{\partial c_p}\delta c_p^{(i)} Y_{1i}(\hat{\boldsymbol{n}})\right\} W(\hat{\boldsymbol{n}}), \quad (28)$$

where $W(\hat{\boldsymbol{n}})$ is a window function for the mask, which can be decomposed into spherical harmonics as

$$W(\hat{\boldsymbol{n}}) = \sum_{\ell m} w_{\ell m}\, Y_{\ell m}(\hat{\boldsymbol{n}}). \quad (29)$$

Since $W(\hat{\boldsymbol{n}})$ is a real-valued function, this implies that $w^*_{\ell m} = (-1)^m w_{\ell\,-m}$. We deduce from Eqs. (1) and (28) that

$$a_{\ell m} = a_{\ell m}^{\rm masked} + \sum_i \delta c_p^{(i)} A_{\ell m}^{(i)}, \quad (30)$$

where $a_{\ell m}^{\rm masked}$ are the coefficients of the masked primordial temperature field $\Theta^{\rm masked}(\hat{\boldsymbol{n}}) = \bar{\Theta}(\hat{\boldsymbol{n}})W(\hat{\boldsymbol{n}})$,

$$a_{\ell m}^{\rm masked} = \sum_{\ell_1 m_1}\bar{a}_{\ell_1 m_1}\sum_{\ell_2 m_2} w_{\ell_2 m_2} \times \int \mathrm{d}^2\hat{\boldsymbol{n}}\; Y_{\ell_1 m_1}(\hat{\boldsymbol{n}})Y_{\ell_2 m_2}(\hat{\boldsymbol{n}})Y^*_{\ell m}(\hat{\boldsymbol{n}}), \quad (31)$$

and the effects of the modulation are encoded in the correction

$$A_{\ell m}^{(i)} = \sum_{\ell_1 m_1}\frac{\partial\bar{a}_{\ell_1 m_1}}{\partial c_p}\sum_{\ell_2 m_2} w_{\ell_2 m_2} \times \int \mathrm{d}^2\hat{\boldsymbol{n}}\; Y_{\ell_1 m_1}(\hat{\boldsymbol{n}})Y_{\ell_2 m_2}(\hat{\boldsymbol{n}})Y_{1i}(\hat{\boldsymbol{n}})Y^*_{\ell m}(\hat{\boldsymbol{n}}). \quad (32)$$

These results have already been presented in Prunet et al. (2005) to search for a dipole signal in WMAP masked maps; the estimator used in Prunet et al. (2005) was the precursor of the optimal estimator of Hanson & Lewis (2009) that we use in our analysis.

5.2. Optimal estimator

To constrain the effect of a spatial variation of the fundamental constants, we need to adapt the estimator proposed by Hanson & Lewis (2009). For that purpose, we start from Eq. (21), which reads, in terms of harmonic coefficients,

$$a_{\ell m} \simeq a_{\ell m}^{\rm masked} + \sum_p\sum_{LM}\sum_i \frac{\partial\bar{a}_{LM}}{\partial c_p}\delta c_p^{(i)}\int \mathrm{d}^2\hat{\boldsymbol{n}}\, Y^*_{\ell m}(\hat{\boldsymbol{n}})Y_{LM}(\hat{\boldsymbol{n}})Y_{1i}(\hat{\boldsymbol{n}}), \quad (33)$$

where, unlike Eq. (22), we do not evaluate the integral over the sky, but over a window function, as we are working on a masked sky. This allows us to compute the covariance matrix $C_{\ell_1 m_1,\ell_2 m_2} \equiv \langle a_{\ell_1 m_1} a^*_{\ell_2 m_2}\rangle$ to first order in $\delta c_p^{(i)}$:

$$C_{\ell_1 m_1,\ell_2 m_2} = \delta_{\ell_1\ell_2}\delta_{m_1 m_2}C_{\ell_1} + \frac{1}{2}\sum_p\sum_i \delta c_p^{(i)}\left[\frac{\partial C_{\ell_1}}{\partial c_p}+\frac{\partial C_{\ell_2}}{\partial c_p}\right] \times \int \mathrm{d}^2\hat{\boldsymbol{n}}\, Y_{1i}(\hat{\boldsymbol{n}})Y^*_{\ell_1 m_1}(\hat{\boldsymbol{n}})Y_{\ell_2 m_2}(\hat{\boldsymbol{n}}). \quad (34)$$

It follows that the unnormalized quadratic maximum likelihood (QML) estimator proposed by Hanson & Lewis (2009) takes the form

$$\widetilde{\delta c_p^{(i)}} = \sum_p \int \mathrm{d}^2\hat{\boldsymbol{n}}\, Y^*_{1i}(\hat{\boldsymbol{n}})\left[\sum_{\ell_1 m_1}\underline{a}_{\ell_1 m_1}Y_{\ell_1 m_1}(\hat{\boldsymbol{n}})\right] \times\left[\sum_{\ell_2 m_2}\frac{1}{2}\frac{\partial C_{\ell_2}}{\partial c_p}\underline{a}_{\ell_2 m_2}Y_{\ell_2 m_2}(\hat{\boldsymbol{n}})\right], \quad (35)$$

where we have introduced the data weighted by the inverse of the covariance,

$$\underline{a}_{\ell m} = \sum_{\ell' m'}(C^{-1}_{\rm obs})_{\ell m\ell' m'}a_{\ell' m'}. \quad (36)$$

Even with a mask, one can use the full-sky approximation in which $C^{-1}_{\rm obs} \simeq 1/(C_\ell b_\ell^2 + N_\ell)$, where C_ℓ is the angular power spectrum of the CMB, b_ℓ^2 is the beam, and N_ℓ is the power spectrum of the noise. However, we emphasize here that even in an ideal case (i.e., no noise and no mask), this estimator is biased; we will show below how to eliminate the bias using simulations.

In the following sub-sections, we restrict the study to a single varying constant, the fine structure constant α, so that $c_p = \alpha$. We assume that this constant has a dipole pattern around our last-scattering surface, but no monopole.

5.3. Simulation of maps without a modulated signal

In order to calibrate the estimators described above, we need to simulate CMB maps with and without a modulation of the fine structure constant. We first describe the simulations produced without any modulation.

The spherical harmonic decomposition reads

$$\bar{\Theta}(\hat{\boldsymbol{n}}) = \sum_{\ell m}\bar{a}_{\ell m}Y_{\ell m}(\hat{\boldsymbol{n}}) = \sum_{\ell m}\sqrt{C_\ell}\epsilon_{\ell m}Y_{\ell m}(\hat{\boldsymbol{n}}) \quad (37)$$

for the isotropic map, where $\epsilon_{\ell m}$ is an $\mathcal{N}(0,1)$ complex Gaussian random variable.

We generated synthetic maps with a Gaussian beam of full width half maximum 5′, which is the resolution of the foreground-cleaned *Planck* CMB maps

(Planck Collaboration XII 2014). The corresponding noise realizations were obtained from realistic simulations of the noise of each individual *Planck* frequency map (including noise correlations in the timelines, and anisotropic sky coverage), which were propagated through the component separation filters. These should therefore faithfully sample the noise covariance of the CMB foreground-cleaned map.

In order to minimize the impact of foreground residual emission from the Galaxy, we adopted the CG80 mask (combined Galactic mask with 80% sky coverage) from Planck Collaboration XII (2014). To minimize artificial mode coupling induced by the mask, we apodized it with a cosine of 8° width. We also attempted to include an additional point source mask (with or without a 30′ apodization). However, in this case, we noticed that instabilities rise in the Hanson & Lewis estimator at large multipoles. Therefore, when building the estimator, we decided to mask the Galaxy, but to "inpaint" the *Planck* CMB map inside the point source mask with constrained Gaussian realizations, as was done in the CMB lensing analysis of Planck Collaboration XVII (2014). In the present study, we have not quantified precisely the influence of the size and type of the mask; this would require considerable additional computations, which would certainly be important if a signal was to be detected. But in any case, there is no reason to believe that the mask effects are substantially different from related studies (e.g., Planck Collaboration XXVII 2014).

5.4. Simulation of maps with a modulated signal

We simulated a *Planck*-like map with a dipole variation of α, starting from the previous modulation-free CMB realizations. For this purpose, we used Eq. (21), which describes the Taylor expansion of the CMB temperature anisotropies in the presence of a dipolar variation of α. Now, let us consider the harmonic decomposition of $\frac{\partial\bar{\Theta}(\hat{\boldsymbol{n}})}{\partial\alpha}$. Given Eq. (37), we obtain

$$\frac{\partial\bar{\Theta}(\hat{\boldsymbol{n}})}{\partial\alpha} = \sum_{\ell m}\frac{\partial\sqrt{C_\ell}}{\partial\alpha}\epsilon_{\ell m}Y_{\ell m}(\hat{\boldsymbol{n}}) = \sum_{\ell m}\frac{1}{2C_\ell}\frac{\partial C_\ell}{\partial\alpha}\bar{a}_{\ell m}Y_{\ell m}(\hat{\boldsymbol{n}}). \quad (38)$$

Using Eqs. (21), (37), and (38) it is thus straightforward to generate a synthetic CMB map with a dipole modulation in α, starting from the unmodulated maps described in Sect. 5.3.

5.5. Calibration of the Hanson-Lewis estimator

We have defined an estimator that allows us to constrain a dipolar spatial variation of the fine structure constant. As explained above, this estimator is expected to be biased, especially in the presence of a mask.

Therefore, in order to eliminate this bias, we need to subtract the mean field[7], $\langle\widetilde{\delta\alpha^{(i)}}\rangle$, computed from unmodulated simulations, and to renormalize with the help of the normalization matrix $\mathcal{F}$, calculated from modulated simulations, so that

$$\widehat{\delta\alpha^{(i)}} = {\mathcal{F}_{ij}}^{-1}\left(\widetilde{\delta\alpha^{(j)}} - \langle\widetilde{\delta\alpha^{(j)}}\rangle\right). \quad (39)$$

The matrix $\mathcal{F}$ corresponds to the 3×3 Fisher matrix of the $\delta\alpha^{(i)}$ coefficients, at least in the case where the data are precisely inverse covariance weighted (see Eq. (36)). We can understand it as the inverse covariance of the estimator in the ideal case without modulation ($\mathcal{F}^{-1}_{\text{no mod}} \simeq \sigma^2$).

[7] Here, $\langle\rangle$ indicate the ensemble average in the absence of modulation.

Let us define an orthonormal basis $(\hat{x},\hat{y},\hat{z})$ for our sky maps. Here $\hat{x}$ and $\hat{y}$ are two orthonormal vectors lying in the Galactic equatorial plane and $\hat{z}$ is the vector normal to this plane. The term $\mathcal{F}_{00}$ strongly depend on the shape of the mask in the $\hat{z}$ direction, whereas $\mathcal{F}_{11}$ and $\mathcal{F}_{-1-1}$ depends on the shape of the mask in the $\hat{x}$ and $\hat{y}$ directions. The terms $\mathcal{F}_{11}$ and $\mathcal{F}_{-1-1}$ are quite similar, but not exactly the same ($\mathcal{F}_{11} = \mathcal{F}_{-1-1}$ only for a simple azimuthal mask). We expect $\mathcal{F}_{11}$ and $\mathcal{F}_{-1-1}$ to be smaller than $\mathcal{F}_{00}$: more information is lost in the $(\hat{x},\hat{y})$ plane because it is aligned with the Galactic plane mask, and it is more difficult to recover these modulation components than in the $\hat{z}$ direction.

In order to determine the mean field and the $\mathcal{F}$ matrix, we started by generating a set of 900 realizations of CMB temperature maps (without dipolar modulation) at a `HEALPix` (Gorski et al. 2005) resolution of $N_{\text{side}} = 2048$. We then added noise and a Galactic mask to these maps, as described in Sect. 5.3.

We used 500 of these unmodulated simulations to estimate the mean field term by calculating the biased estimator $\widetilde{\delta\alpha^{(i)}}$ for each of these maps and by performing the ensemble average over these values.

We then used the remaining 400 unmodulated maps to produce different sets of modulated simulations, as explained in Sect. 5.4, in order to determine the elements of $\mathcal{F}$. In particular, to determine the first column $\mathcal{F}_{i0}$ of the matrix $\mathcal{F}$ we simulated 400 maps with a fiducial modulation $\delta\alpha^{(0)} = 0.1$, with all other components $\mathrm{Re}(\delta\alpha^{(1)})$ and $\mathrm{Im}(\delta\alpha^{(1)})$ set to zero. We estimate the first column $\mathcal{F}_{i0}$ from the ensemble average of Eq. (41):

$$\mathcal{F}_{i0} = \frac{1}{\langle\widehat{\delta\alpha^{(0)}}\rangle}\mathcal{F}\begin{pmatrix}\langle\widehat{\delta\alpha^{(0)}}\rangle\\0\\0\end{pmatrix} \quad (40)$$

$$= \frac{1}{\langle\widehat{\delta\alpha^{(0)}}\rangle}\begin{pmatrix}\langle\widetilde{\delta\alpha^{(0)}}\rangle_{\text{mod}} - \langle\widetilde{\delta\alpha^{(0)}}\rangle\\ \mathrm{Re}\left(\langle\widetilde{\delta\alpha^{(1)}}\rangle_{\text{mod}} - \langle\widetilde{\delta\alpha^{(1)}}\rangle\right)\\ \mathrm{Im}\left(\langle\widetilde{\delta\alpha^{(1)}}\rangle_{\text{mod}} - \langle\widetilde{\delta\alpha^{(1)}}\rangle\right)\end{pmatrix}. \quad (41)$$

Here $\widetilde{\delta\alpha^{(0)}}$ is the biased estimator calculated on each of the modulated simulations, $\langle\widehat{\delta\alpha^{(0)}}\rangle$ is the previously calculated mean field, and the expected value of the ensemble average of the unbiased estimator $\langle\widehat{\delta\alpha}^{(0)}\rangle$ is assumed to correspond to the input fiducial value of the simulations. We similarly determine $\mathcal{F}_{i1}$ and $\mathcal{F}_{i-1}$, assuming as a fiducial $\mathrm{Re}(\delta\alpha^{(1)}) = 0.1$ or $\mathrm{Im}(\delta\alpha^{(1)}) = 0.1$, respectively, with all other components set to zero. We report only the diagonal elements of the obtained $\mathcal{F}$ matrix in Table 6, although we use the full matrix in our analysis .

After that, we used all the 900 unmodulated simulations in order to determine the variance of the estimator. For each of these simulations, we estimate $\widehat{\delta\alpha^{(0)}}$ and the real and imaginary parts of $\widehat{\delta\alpha^{(1)}}$. The histogram of these values are shown in Fig. 10, while Table 6 lists the results for the mean field, the $\mathcal{F}_{ii}$ elements, and the variance of the estimator for two specific choices of the maximum multipole included in the analysis, $\ell_{\text{max}} = 600$ and $\ell_{\text{max}} = 1500$. We notice that the high multipoles contribute considerably in decreasing the variance of the different $\delta\alpha^{(i)}$ components, by up to a factor 5 for $\ell_{\text{max}} = 1500$ compared to the $\ell_{\text{max}} = 600$ case (as expected, since the number of modes grows like ℓ^2_{max}).

Finally, let us focus on the amplitude of the modulation $\widetilde{\delta\alpha} = \frac{1}{2}\sqrt{\frac{3}{\pi}}\sqrt{|\widehat{\delta\alpha^{(0)}}|^2 + 2\left|\widehat{\delta\alpha^{(1)}}\right|^2}$, as already defined in Eq. (18). This quantity is interesting as it reveals the presence of a dipole regardless of its direction. Although calculated from the

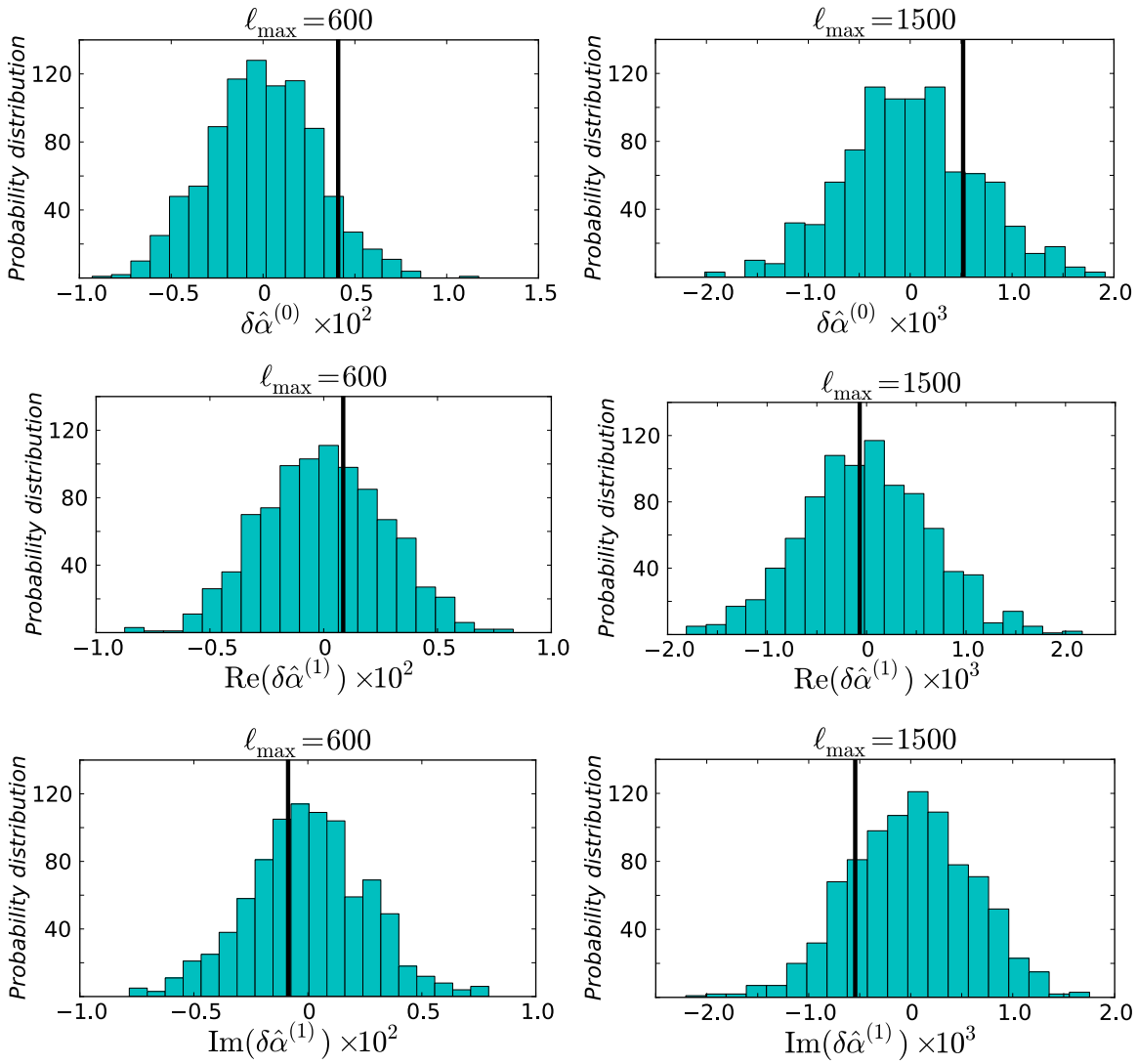

Fig. 10. *Left*: histogram of the distribution of the components of the dipole modulation for 900 unmodulated realizations. The distribution is not normalized. *From top to bottom* we show $\delta\alpha^{(0)}$, $\mathrm{Re}(\delta\alpha^{(1)})$ and $\mathrm{Im}(\delta\alpha^{(1)})$. The three histograms correspond to *Planck*-like modulation-free simulated data with $\ell_{\rm max}=600$. The black line corresponds to the measurements in the actual *Planck* CMB map. *Right*: the same thing for $\ell_{\rm max}=1500$.

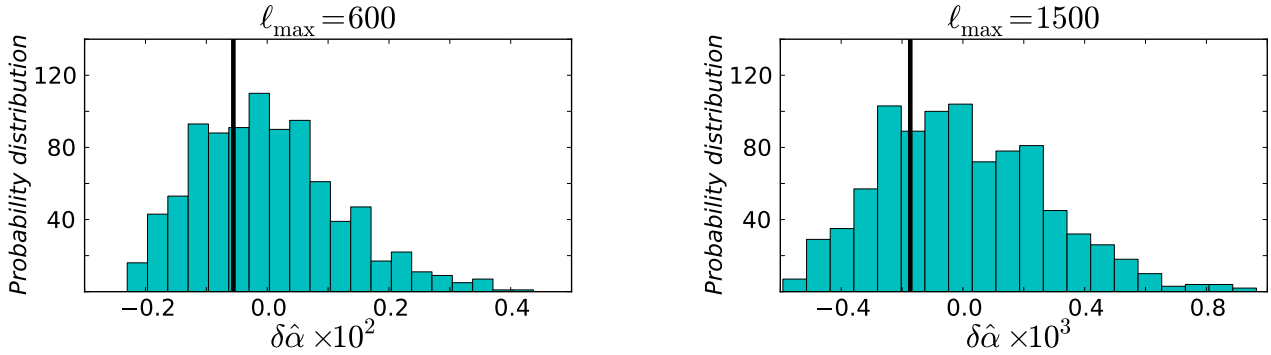

Fig. 11. Histogram of the distribution of the overall amplitude of the dipole modulation for 900 unmodulated realizations. The distribution is not normalized. The histogram on the left corresponds to *Planck*-like simulated data without modulation with $\ell_{\rm max}=600$, while the one on the right os for $\ell_{\rm max}=1500$. In each plot, the black line corresponds to the measurements in the actual *Planck* CMB map.

unbiased $\delta\alpha^{(i)}$ components, this quantity is still biased. To correct for this, we subtract an additional mean field term $\langle\widetilde{\delta\alpha}\rangle$, computed from 500 unmodulated realizations, in order to obtain the unbiased amplitude $\widehat{\delta\alpha}=\widetilde{\delta\alpha}-\langle\widetilde{\delta\alpha}\rangle$. Table 7 summarizes the variance and the mean field of the amplitude.

As a final cross-check, we simulated maps, with the appropriate angular resolution, noise content and mask, for different fiducial modulations, and check whether we recover the input value using our unbiased estimator. We consider the following nine fiducial cases: $\delta\alpha^{(0)}\in\{10^{-1},10^{-2},10^{-3}\}$ with all the

Table 6. Mean fields (computed with 500 realizations of modulation-free *Planck*-like maps), variances (computed by estimating dipole components on 900 realizations of modulation-free *Planck*-like maps) and diagonal elements of $\mathcal{F}$ (computed with 400 realizations of modulated *Planck*-like maps) of each component of the modulation for the Hanson & Lewis (2009) estimator with $\ell_{\rm max} = 600$ and $\ell_{\rm max} = 1500$.

Quantities		$\ell_{\rm max} = 600$	$\ell_{\rm max} = 1500$
Variances	$\sigma_{\delta\alpha^{(0)}}$	2.95×10^{-3}	6.50×10^{-4}
	$\sigma_{{\rm Re}(\delta\alpha^{(1)})}$	2.70×10^{-3}	6.45×10^{-4}
	$\sigma_{{\rm Im}(\delta\alpha^{(1)})}$	2.61×10^{-3}	5.97×10^{-4}
Mean fields	$\mathcal{F}^{-1}\langle\widetilde{\delta\alpha^{(0)}}\rangle$	5.93×10^{-3}	4.57×10^{-3}
	$\mathcal{F}^{-1}\langle{\rm Re}(\widetilde{\delta\alpha^{(1)}})\rangle$	-1.50×10^{-2}	-7.97×10^{-3}
	$\mathcal{F}^{-1}\langle{\rm Im}(\widetilde{\delta\alpha^{(1)}})\rangle$	-1.84×10^{-2}	-9.46×10^{-3}
Diagonal elements of $\mathcal{F}$ . . .	$\mathcal{F}_{00}$	3.24×10^{5}	1.67×10^{8}
	$\mathcal{F}_{11}$	1.75×10^{5}	9.08×10^{7}
	$\mathcal{F}_{-1-1}$	2.00×10^{5}	1.04×10^{8}

other coefficients equal to zero, ${\rm Re}(\delta\alpha^{(1)}) \in \{10^{-1}, 10^{-2}, 10^{-3}\}$ with all the other coefficients equal to zero, and ${\rm Im}(\delta\alpha^{(1)}) \in \{10^{-1}, 10^{-2}, 10^{-3}\}$ with all the other coefficients equal to zero. We apply the unbiased estimator on these maps and check that in all nine cases considered we recover the input value of the different components $\delta\alpha^{(i)}$ and the amplitude $\delta\alpha$ within 3σ.

We consider two values of $\ell_{\rm max}$, in order to determine how much the high multipoles contribute to improve the estimates. The first, $\ell_{\rm max} = 600$, roughly corresponds to the $\ell_{\rm max}$ at which a modulation with $|\delta\alpha^{(i)}| \approx 10^{-1}$ (i.e., a dipolar modulation of amplitude $\delta\alpha \approx 10^{-2}$) is well detected at more than 10σ from the unmodulated distribution. The second value, $\ell_{\rm max} = 1500$, still corresponds to the signal-dominated regime of *Planck* and is roughly the $\ell_{\rm max}$ at which a modulation with $|\delta\alpha^{(i)}| \approx 10^{-2}$ (i.e., a dipolar modulation of amplitude $\delta\alpha \approx 10^{-3}$) is well detected at more than 10σ from the unmodulated distribution. However, for $|\delta\alpha^{(i)}| \approx 10^{-3}$, the estimates can no longer be easily distinguished from the unmodulated case. We note that for *Planck* at $\ell_{\rm max} > 1500$, the rising noise cancels the benefit of adding more modes.

5.6. Results on data

We finally apply the unbiased Hanson-Lewis estimator to the *Planck* data. More specifically, we use the CMB foreground-cleaned SMICA map (Planck Collaboration XII 2014), which shares the same resolution and noise covariance as the *Planck* simulations used above. The results are shown in Table 8, for $\ell_{\rm max} = 600$ and $\ell_{\rm max} = 1500$. All the components of the dipolar modulation of the fine structure constant are compatible with zero at the 1σ level, except for $\widehat{\delta\alpha^{(0)}}$ at $\ell_{\rm max} = 600$, which is still compatible with zero within 2σ. At the 1σ level, the overall amplitude of the modulation is also compatible with zero. There is thus no detection of a dipole modulation in the fine structure constant in the *Planck* data. Dividing by the standard value of the fine structure constant, α_0, the results on the amplitude reported in Table 8 correspond to $\widehat{\delta\alpha}/\alpha_0 = (-8 \pm 16) \times 10^{-2}$ for $\ell_{\rm max} = 600$ and $\widehat{\delta\alpha}/\alpha_0 = (-2.4 \pm 3.7) \times 10^{-2}$ for $\ell_{\rm max} = 1500$ at 68% CL.

6. Summary and conclusions

We have provided a detailed analysis of the variation of two fundamental constants, the fine structure constant α and the mass of the electron $m_{\rm e}$, on the CMB angular power spectra. We have presented the constraints that can be derived from the recent *Planck* data, focusing on these two constants because they are the ones that mostly affect the cosmic recombination process.

Table 7. Mean field $\langle\widetilde{\delta\alpha}\rangle$ and variance $\sigma_\alpha^2 = \langle\delta\alpha^2\rangle - \langle\delta\alpha\rangle^2$ of the amplitude $\delta\alpha$ of the modulation for 900 *Planck* realizations of the Hanson & Lewis (2009) estimator for the specific choices $\ell_{\rm max} = 600$ and $\ell_{\rm max} = 1500$.

Hanson-Lewis estimator	$\ell_{\rm max} = 600$	$\ell_{\rm max} = 1500$
Variances $\sigma_{\delta\alpha}$	1.17×10^{-3}	2.71×10^{-4}
Mean fields $\langle\widetilde{\delta\alpha}\rangle$	2.72×10^{-3}	6.29×10^{-4}

As time as variations are concerned, we find that *Planck* data improve the constraints on α/α_0, with respect to those from WMAP-9, by a factor of about 5. Our analysis of *Planck* data limits any variation in the fine-structure constant from $z \sim 10^3$ to the present day to be less than approximately 0.4%, specifically $\alpha/\alpha_0 = 0.9934 \pm 0.0042$ (68% CL) from *Planck*+WP data. We emphasize that *Planck* allows one to break the degeneracy between α and H_0 from the observation of the damping tail. Furthermore, we stress that the 1.6σ deviation of α/α_0 from unity when considering the *Planck*+WP case is strongly reduced when we remove the low-ℓ data, so that this mild deviation is probably coming from the low versus high ℓ tension.

We have also explored how much the constraint on α is weakened by opening up the parameter space to variations of the number of relativistic species or the helium abundance. We find that the constraint on the fine structure constant weakens by about a factor of 1.5 when $N_{\rm eff}$ is allowed to float, while it weakens by up to a factor of 4 when the helium abundance is allowed to float.

As the variation of the mass of the electron is concerned, we find that the constraint from *Planck* is comparable to the one obtained from the WMAP-9 data, namely $m_{\rm e}/m_{\rm e0} = 0.977^{+0.055}_{-0.070}$. This is due to the fact that $m_{\rm e}$ only weakly affects the damping tail, unlike α. Therefore, the degeneracy between $m_{\rm e}$ and H_0 is not broken by observing the high multipoles, and that limits the constraint on $m_{\rm e}$. This degeneracy can be alleviated by adding other data sets; typically, *Planck* data combined with BAO provide a constraint on $m_{\rm e}$ at the 1% level.

The *Planck* data also permit us to set constraints on α and $m_{\rm e}$ when they are both allowed to vary. We find that the constraints on each of the two constants are only slightly weakened, namely

Table 8. Summary of the results obtained for the amplitude of the spatial modulation of the fine structure constant with the Hanson & Lewis Hanson & Lewis (2009) estimator applied to the *Planck* data for $\ell_{\rm max} = 600$ and $\ell_{\rm max} = 1500$. We show uncertainties at 68% CL.

Planck results	$\ell_{\rm max} = 600$	$\ell_{\rm max} = 1500$
$\widehat{\delta\alpha}$	$-5.56 \times 10^{-4} \pm 1.17 \times 10^{-3}$	$-1.73 \times 10^{-4} \pm 2.71 \times 10^{-4}$
$\widehat{\delta\alpha^{(0)}}$	$4.09 \times 10^{-3} \pm 2.95 \times 10^{-3}$	$5.20 \times 10^{-4} \pm 6.50 \times 10^{-4}$
$\mathrm{Re}(\widehat{\delta\alpha^{(1)}})$	$8.57 \times 10^{-4} \pm 2.70 \times 10^{-3}$	$-6.93 \times 10^{-5} \pm 6.45 \times 10^{-4}$
$\mathrm{Im}(\widehat{\delta\alpha^{(1)}})$	$-8.66 \times 10^{-4} \pm 2.61 \times 10^{-3}$	$-5.44 \times 10^{-4} \pm 5.97 \times 10^{-4}$

$\alpha/\alpha_0 = 0.993 \pm 0.0045$ and $m_{\rm e}/m_{\rm e0} = 0.994 \pm 0.059$. In Appendix B we have presented a detailed analysis of the signature of the variation of each constant in order to explain how the observation of the damping tail allows one to break the degeneracy between them.

Concerning spatial variations, we have constrained a dipolar modulation of the fine structure constant. Such a modulation induces mode couplings, and we have presented an estimator that allows one to constrain this effect. The main difficulty is to circumvent the effect of the masking. We performed 900 numerical simulations to calibrate our estimators in order to demonstrate that the *Planck* data set a constraint on the amplitude of such a modulation of $\delta\alpha/\alpha_0 = (-2.4 \times \pm 3.7) \times 10^{-2}$ (68% CL), using multipoles up to $\ell_{\rm max} = 1500$. The conclusion of the analysis is summarized in Table 8.

From a theoretical point of view, our analysis relies on a modified version of the `RECFAST` code. It would be interesting to compare these results with those using more sophisticated (although computationally slower) recombination codes such as `Hyrec` (Ali-Haïmoud & Hirata 2011) and `Cosmorec` (Chluba & Thomas 2011). This would enable us to quantify the accuracy of the description of the recombination process and its effect on the constraints; although the major effect on recombination is through the scaling of the energy levels in hydrogen, it will be worth checking for more subtle effects, in particular when the primordial helium fraction is considered as a free parameter. There is also the possibility of studying the effects of the variations of other constants, such as the mass of the baryons (induced by radiative corrections as soon as α is allowed to vary) or the strength of gravity. The investigation of these possibilities, which requires consideration of specific self-consistent theoretical models are postponed to future work. Similarly, the comparison of the limits derived in this work with the ones obtained at lower redshifts require one to specify a model, since the constraints are very sensitive to the functional form of the time variation of the fundamental constants.

In conclusion, the angular resolution and sensitivity of *Planck* enables us to reach higher accuracy and lift existing degeneracies. Further improvement in studies of both temporal and spatial variation can be expected in the near future by including polarization data from *Planck*, as well as other experiments, such as SPTpol (Austermann et al. 2012), ACTpol (Niemack et al. 2010), and Polarbear (Kermish et al. 2012).

Acknowledgements. The development of *Planck* has been supported by: ESA; CNES and CNRS/INSU-IN2P3-INP (France); ASI, CNR, and INAF (Italy); NASA and DoE (USA); STFC and UKSA (UK); CSIC, MICINN, J.A., and RES (Spain); Tekes, AoF, and CSC (Finland); DLR and MPG (Germany); CSA (Canada); DTU Space (Denmark); SER/SSO (Switzerland); RCN (Norway); SFI (Ireland); FCT/MCTES (Portugal); and PRACE (EU). A description of the Planck Collaboration and a list of its members, including the technical or scientific activities in which they have been involved, can be found at `http://www.sciops.esa.int/index.php?project=planck&page=Planck_Collaboration`. Some of the results in this paper have been derived using the `HEALPix` package. We thank Alain Coc and Elisabeth Vangioni for discussions and S. Rouberol for running the `horizon` cluster, where some of the computations were performed. Some of this work was carried out at the ILP LABEX (under reference ANR-10-LABX-63) and was supported by French state funds managed by the ANR within the Investissements d'Avenir programme under reference ANR-11-IDEX-0004-02 and by the ANR VACOUL. This work was made possible thanks to the ANR Chaire d'Excellence ANR-10-CEXC-004-01.

References

Ali-Haïmoud, Y., & Hirata, C. M. 2011, Phys. Rev. D, 83, 043513
Anderson, L., Aubourg, E., Bailey, S., et al. 2013, MNRAS, 428, 1036
Austermann, J. E., Aird, K. A., Beall, J. A., et al. 2012, SPIE Conf. Ser., 8452
Avelino, P., Martins, C., & Rocha, G. 2000, Phys. Rev. D, 62, 123508
Avelino, P., Esposito, S., Mangano, G., & Martins, C., et al. 2001, Phys. Rev. D, 64, 103505
Aver, E., Olive, K. A., Porter, R. L., & Skillman, E. D. 2013, J. Cosmol. Astropart. Phys., 11, 17
Battye, R., Crittenden, R., & Weller, J. 2001, Phys. Rev. D, 63, 043505
Bennett, C. L., Larson, D., Weiland, J. L., et al. 2013, ApJS, 208, 20
Berengut, J., Flambaum, V., King, J., Curran, S., & Webb, J. 2011, Phys. Rev. D, 83, 123506
Bergström, L., Iguri, S., & Rubinstein, H. 1999, Phys. Rev. D, 60, 045005
Beutler, F., Blake, C., Colless, M., et al. 2011, MNRAS, 416, 3017
Bize, S., Diddams, S., Tanaka, U., et al. 2003, Phys. Rev. Lett., 90, 150802
Bonifacio, P., Rahmani, H., Whitmore, J. B., et al. 2014, Astron. Nachr., 335, 83
Cameron, E., & Pettitt, T. 2012, MNRAS, submitted [arXiv:1207.6223]
Cameron, E., & Pettitt, T. 2013, MNRAS, submitted [arXiv:1309.2737]
Carilli, C. L., Menten, K. M., Stocke, J. T., et al. 2001, Phys. Rev. Lett., 85, 5511
Chluba, J., & Thomas, R. M. 2011, MNRAS, 412, 748
Cingöz, A., Lapierre, A., Nguyen, A.-T., et al. 2008, Phys. Rev. Lett., 98, 040801
Coc, A., Olive, K. A., Uzan, J.-P., & Vangioni, E. 2006, Phys. Rev. D, 73, 083525
Coc, A., Nunes, N. J., Olive, K. A., Uzan, J.-P., & Vangioni, E. 2007, Phys. Rev. D, 76, 023511
Coc, A., Ekström, S., Descouvemont, P., et al. 2009, Mem. Soc. Astron. It., 80, 809
Coc, A., Descouvemont, P., Uzan, J.-P., & Vangioni, E. 2012, PoS, NICXII, 073
Damour, T., & Dyson, F. 1996, Nucl. Phys. B, 480, 37
Damour, T., & Pichon, B. 1999, Phys. Rev. D, 59, 123502
Das, S., Louis, T., Nolta, M. R., et al. 2014, JCAP, 04, 014
Dicke, R. 1964, in Relativity, Groups and Topology. Relativité, Groupes et Topologie, eds. C. DeWitt, & B. DeWitt (New York; London: Gordon and Breach), 165
Dicke, R. H. 1962, Phys. Rev., 125, 2163
Duff, M. J. 2002, ArXiv e-prints [arXiv:hep-th/0208093]
Dyson, F. 1972, in Aspects of Quantum Theory, eds. A. Salam, & E. Wigner (Cambridge; New York: Cambridge University Press), 213
Ekström, S., Coc, A., Descouvemont, P., et al. 2010, A&A, 514, A62
Ellis, G. F., & Uzan, J.-P. 2005, Am. J. Phys., 73, 240
Flambaum, V. V. 2007, Int. J. Mod. Phys. A, 22, 4937
Fujii, Y., Iwamoto, A., Fukahori, T., et al. 2000a, Nucl. Phys. B, 573, 377
Galli, S. 2013, Phys. Rev. D, 87, 123516
Galli, S., Melchiorri, A., Smoot, G. F., & Zahn, O. 2009, Phys. Rev. D, 80, 023508
Galli, S., Martinelli, M., Melchiorri, A., et al. 2010, Phys. Rev. D, 82, 123504
Gelman, A., & Rubin, D. 1992, Statist. Sci., 7, 457
Gorski, K. M., Hivon, E., Banday, A., et al. 2005, ApJ, 622, 759

Gould, C., Sharapov, E., & Lamoreaux, S. 2006, Phys. Rev. C, 74, 024607
Hamann, J., Hannestad, S., Raffelt, G. G., & Wong, Y. Y. 2011, JCAP, 1109, 034
Hannestad, S. 1999, Phys. Rev. D, 60, 023515
Hanson, D., & Lewis, A. 2009, Phys. Rev. D, 80, 063004
Hinshaw, G., Larson, D., Komatsu, E., et al. 2013, ApJS, 208, 19
Hou, Z., Keisler, R., Knox, L., Millea, M., & Reichardt, C. 2013, Phys. Rev. D, 87, 083008
Hu, W., & Sugiyama, N. 1995, ApJ, 444, 489
Ichikawa, K., Kanzaki, T., & Kawasaki, M. 2006, Phys. Rev. D, 74, 023515
Jain, B., Joyce, A., Thompson, R., et al. 2013, ArXiv e-prints [arXiv:1309.5389]
Kaiser, N. 1983, MNRAS, 202, 1169
Kanekar, N., Carilli, C. L., Langston, C. I., et al. 2005, Phys. Rev. Lett., 95, 261301
Kaplinghat, M., Scherrer, R., & Turner, M. 1999, Phys. Rev. D, 60, 023516
Kermish, Z. D., Ade, P., Anthony, A., et al. 2012, SPIE Conf. Ser., 8452
King, J. A., Webb, J. K., Murphy, M. T., et al. 2012, MNRAS, 422, 3370
Kuroda, P. 1956, J. Chem. Phys., 25, 781
Landau, S., & Scóccola, C. 2010, A&A, 517, A62
Landau, S., Harari, D., & Zaldarriaga, M. 2001, Phys. Rev. D, 63, 083505
Lewis, A., & Bridle, S. 2002, Phys. Rev., D66, 103511
Livio, M., Hollowell, D., Weiss, A., & Truran, J. 1989, Nature, 340, 281
Luo, F., Olive, K. A., & Uzan, J.-P. 2011, Phys. Rev. D, 84, 096004
Martins, C. J. A. P. 2003, Astrophys. Space Sci., 283, 439
Martins, C., Melchiorri, A., Rocha, G., et al. 2004a, Phys. Lett. B, 585, 29
Martins, C. J. A. P., Melchiorri, A., Rocha, G., & Trotta, R., et al. 2004b, Phys. Lett. B, 585, 29
Menegoni, E. 2010, AIP Conf. Proc., 1256, 288
Menegoni, E., Galli, S., Bartlett, J., Martins, C., & Melchiorri, A. 2009, Phys. Rev. D, 80, 087302
Menegoni, E., Archidiacono, M., Calabrese, E., et al. 2012, Phys. Rev. D 85, 107301
Mohr, P., Taylor, B., & Newell, D. 2008, Rev. Mod. Phys., 80, 633
Moss, A., Scott, D., Zibin, J. P., & Battye, R. 2011, Phys. Rev. D, 84, 023014
Mukhanov, V., Kim, J., Naselsky, P., Trombetti, T., & Burigana, C. 2012, JCAP, 1206, 040
Müller, C. M., Schäfer, G., & Wetterich, C. 2004, Phys. Rev. D, 70, 083504
Nakashima, M., Nagata, R., & Yokoyama, J. 2008, Prog. Theor. Phys., 120, 1207
Nakashima, M., Ichikawa, K., Nagata, R., & Yokoyama, J. 2010, JCAP, 1001, 030
Narimani, A., Moss, A., & Scott, D. 2012, Ap&SS, 341, 617
Niemack, M. D., Ade, P. A. R., Aguirre, J., et al. 2010, SPIE Conf. Ser., 7741
O'Bryan, J., Smidt, J., De Bernardis, F., & Cooray, A. 2013, PRL, submitted [arXiv:1306.1232]
Olive, K. A., & Pospelov, M. 2002, Phys. Rev. D, 65, 085044
Olive, K., Pospelov, M., Qian, Y.-Z., et al. 2002, Phys. Rev. D, 66, 045022
Olive, K. A., Peloso, M., & Uzan, J.-P. 2011, Phys. Rev. D, 83, 043509
Olive, K. A., Peloso, M., & Peterson, A. J. 2012, Phys. Rev. D, 86, 043501
Padmanabhan, N., Xu, X., Eisenstein, D. J., et al. 2012, MNRAS, 427, 2132
Peik, E., Lipphardt, B., Schnatz, H., et al. 2008, in The Eleventh Marcel Grossmann Meeting on General Relativity, eds. H. Kleinert, R. Jantzen, & R. Ruffini (Singapore; Hackensack, NJ: World Scientific), 941
Péquignot, D., Petitjean, P., & Boisson, C. 1991, A&A, 251, 680
Pisanti, O., Cirillo, A., Esposito, S., et al. 2008, Comput. Phys. Commun., 178, 956
Pitrou, C., Uzan, J.-P., & Bernardeau, F. 2008, Phys. Rev., D 78, 063526
Planck Collaboration I. 2014, A&A, 571, A1
Planck Collaboration XII. 2014,A&A, 571, A12
Planck Collaboration XV. 2014, A&A, 571, A15
Planck Collaboration XVI. 2014, A&A, 571, A16
Planck Collaboration XVII. 2014, A&A, 571, A17
Planck Collaboration XXVII. 2014, A&A, 571, A27
Prunet, S., Uzan, J.-P., Bernardeau, F., & Brunier, T. 2005, Phys. Rev. D, 71, 083508
Reichardt, C. L., Shaw, L., Zahn, O., et al. 2012, ApJ, 755, 70
Riazuelo, A., & Uzan, J.-P. 2002, Phys. Rev. D, 66, 023525
Riess, A. G., Macri, L., Casertano, S., et al. 2011, ApJ, 730, 119
Rocha, G., Trotta, R., Martins, C., & Melchiorri, A., et al. 2004, MNRAS, 32, 20
Rosenband, T., Hume, D., Schmidt, P., et al. 2008, Science, 319, 1808
Savedoff, M. 1956, Nature, 178, 688
Scoccola, C. G. 2009, Ph.D. Thesis, Universidad Nacional de La Plata, Argentina [arXiv:0906.0329]
Scoccola, C., Landau, S., & Vucetich, H. 2008, Phys. Lett. B, 669, 212
Scoccola, C., Landau, S., & Vucetich, H. 2009, Mem. Soc. Astron. It., 80, 814
Scóccola, C. G., Sánchez, A. G., Rubiño-Martín, J. A., et al. 2013, MNRAS, 434, 1792
Seager, S., Davelov, D. D., & Scott, D. 1999, ApJ, 523, L1
Seager, S., Sasselov, D. D., & Scott, D. 2000, ApJS, 128, 407
Shlyakhter, A. 1976, Nature, 264, 340
Sievers, J. L., Hlozek, R. A., Nolta, M. R., et al. 2013, J. Cosmol. Astropart. Phys., 10, 60
Sigurdson, K., Kurylov, A., & Kamionkowski, M. 2003, Phys. Rev. D., 68, 103509
Silk, J. 1968, ApJ, 151, 459
Srianand, R., Chand, H., Petitjean, P., & Aracil, B. 2004, Phys. Rev. Lett., 92, 121302
Srianand, R., Chand, H., Petitjean, P., & Aracil, B. 2007, Phys. Rev. Lett., 99, 239002
Stefanecsu, P. 2007, New Astron., 12, 635
Uzan, J.-P. 2003, Rev. Mod. Phys., 75, 403
Uzan, J.-P. 2007, Gen. Rel. Grav., 39, 307
Uzan, J.-P. 2011, Liv. Rev. Rel., 14, 2
Webb, J., Murphy, M., Flambaum, V., & Dzuba, V., et al. 2001, Phys. Rev. Lett., 87, 091301
Webb, J., King, J., Murphy, M., et al. 2011, Phys. Rev. Lett., 107, 191101
Wilkinson, D. 1958, Philos. Mag., 3, 582
Will, C. M. 1981, Theory and experiment in gravitational physics (Cambridge University Press)
Wong, W. Y., Moss, A., & Scott, D. 2008, MNRAS, 386, 1023
Zahn, O., & Zaldarriaga, M. 2003, Phys. Rev. D, 67, 063002
Zaldarriaga, M., & Harari, D. D. 1995, Phys. Rev. D, 52, 3276

[1] APC, AstroParticule et Cosmologie, Université Paris Diderot, CNRS/IN2P3, CEA/lrfu, Observatoire de Paris, Sorbonne Paris Cité, 10 rue Alice Domon et Léonie Duquet, 75205 Paris Cedex 13, France
[2] African Institute for Mathematical Sciences, 6−8 Melrose Road, Muizenberg, 7950 Cape Town, South Africa
[3] Agenzia Spaziale Italiana Science Data Center, via del Politecnico snc, 00133 Roma, Italy
[4] Agenzia Spaziale Italiana, viale Liegi 26, 00198 Roma, Italy
[5] Astrophysics Group, Cavendish Laboratory, University of Cambridge, J J Thomson Avenue, Cambridge CB3 0HE, UK
[6] Astrophysics & Cosmology Research Unit, School of Mathematics, Statistics & Computer Science, University of KwaZulu-Natal, Westville Campus, Private Bag X54001, 4000 Durban, South Africa
[7] Atacama Large Millimeter/submillimeter Array, ALMA Santiago Central Offices, Alonso de Cordova 3107, Vitacura, Casilla 763 0355, Santiago, Chile
[8] CITA, University of Toronto, 60 St. George St., Toronto, ON M5S 3H8, Canada
[9] CNRS, IRAP, 9 Av. colonel Roche, BP 44346, 31028 Toulouse Cedex 4, France
[10] California Institute of Technology, Pasadena, CA 91125, USA
e-mail: graca@caltech.edu
[11] Centro de Estudios de Física del Cosmos de Aragón (CEFCA), Plaza San Juan, 1, planta 2, 44001 Teruel, Spain
[12] Computational Cosmology Center, Lawrence Berkeley National Laboratory, Berkeley, CA, USA
[13] Consejo Superior de Investigaciones Científicas (CSIC), 28049 Madrid, Spain
[14] DSM/Irfu/SPP, CEA-Saclay, 91191 Gif-sur-Yvette Cedex, France
[15] DTU Space, National Space Institute, Technical University of Denmark, Elektrovej 327, 2800 Kgs, Lyngby, Denmark
[16] Département de Physique Théorique, Université de Genève, 24 quai E. Ansermet, 1211 Genève 4, Switzerland
[17] Departamento de Física, Universidad de Oviedo, Avda. Calvo Sotelo s/n, 33007 Oviedo, Spain
[18] Department of Astrophysics/IMAPP, Radboud University Nijmegen, PO Box 9010, 6500 GL Nijmegen, The Netherlands
[19] Department of Physics & Astronomy, University of British Columbia, 6224 Agricultural Road, Vancouver, British Columbia, Canada
[20] Department of Physics and Astronomy, Dana and David Dornsife College of Letter, Arts and Sciences, University of Southern California, Los Angeles, CA 90089, USA
[21] Department of Physics and Astronomy, University College London, London WC1E 6BT, UK

[22] Department of Physics, Florida State University, Keen Physics Building, 77 Chieftan Way, Tallahassee, FL, USA
[23] Department of Physics, Gustaf Hällströmin katu 2a, University of Helsinki, Helsinki, Finland
[24] Department of Physics, Princeton University, Princeton, NJ, USA
[25] Department of Physics, University of California, Santa Barbara, CA, USA
[26] Dipartimento di Fisica e Astronomia G. Galilei, Università degli Studi di Padova, via Marzolo 8, 35131 Padova, Italy
[27] Dipartimento di Fisica e Scienze della Terra, Università di Ferrara, via Saragat 1, 44122 Ferrara, Italy
[28] Dipartimento di Fisica, Università La Sapienza, P.le A. Moro 2, Roma, Italy
[29] Dipartimento di Fisica, Università degli Studi di Milano, via Celoria, 16 Milano, Italy
[30] Dipartimento di Fisica, Università degli Studi di Trieste, via A. Valerio 2, Trieste, Italy
[31] Dipartimento di Fisica, Università di Roma Tor Vergata, via della Ricerca Scientifica, 1 Roma, Italy
[32] Discovery Center, Niels Bohr Institute, Blegdamsvej 17 Copenhagen, Denmark
[33] Dpto. Astrofísica, Universidad de La Laguna (ULL), 38206 La Laguna, Tenerife, Spain
[34] European Southern Observatory, ESO Vitacura, Alonso de Cordova 3107, Vitacura, Casilla 19001, Santiago, Chile
[35] European Space Agency, ESAC, Planck Science Office, Camino bajo del Castillo, s/n, Urbanización Villafranca del Castillo, Villanueva de la Cañada, Madrid, Spain
[36] European Space Agency, ESTEC, Keplerlaan 1, 2201 Noordwijk, The Netherlands
[37] Helsinki Institute of Physics, Gustaf Hällströmin katu 2, University of Helsinki, Helsinki, Finland
[38] INAF–Osservatorio Astronomico di Padova, Vicolo dell'Osservatorio 5, Padova, Italy
[39] INAF–Osservatorio Astronomico di Roma, via di Frascati 33, Monte Porzio Catone, Italy
[40] INAF–Osservatorio Astronomico di Trieste, via G.B. Tiepolo 11, Trieste, Italy
[41] INAF/IASF Bologna, via Gobetti 101, Bologna, Italy
[42] INAF/IASF Milano, via E. Bassini 15, Milano, Italy
[43] INFN, Sezione di Bologna, via Irnerio 46, 40126 Bologna, Italy
[44] INFN, Sezione di Roma 1, Università di Roma Sapienza, Piazzale Aldo Moro 2, 00185 Roma, Italy
[45] INFN/National Institute for Nuclear Physics, via Valerio 2, 34127 Trieste, Italy
[46] IPAG: Institut de Planétologie et d'Astrophysique de Grenoble, Université Joseph Fourier, Grenoble 1/CNRS-INSU, UMR 5274, 38041 Grenoble, France
[47] Imperial College London, Astrophysics group, Blackett Laboratory, Prince Consort Road, London, SW7 2AZ, UK
[48] Infrared Processing and Analysis Center, California Institute of Technology, Pasadena, CA 91125, USA
[49] Institut Universitaire de France, 103 bd Saint-Michel, 75005 Paris, France
[50] Institut d'Astrophysique Spatiale, CNRS (UMR 8617) Université Paris-Sud 11, Bâtiment 121, Orsay, France
[51] Institut d'Astrophysique de Paris, CNRS (UMR 7095), 98bis boulevard Arago, 75014 Paris, France
[52] Institute for Space Sciences, Bucharest-Magurale, Romania
[53] Institute of Astronomy, University of Cambridge, Madingley Road, Cambridge CB3 0HA, UK
[54] Institute of Theoretical Astrophysics, University of Oslo, Blindern, Oslo, Norway
[55] Instituto de Astrofísica de Canarias, C/Vía Láctea s/n, La Laguna, Tenerife, Spain
[56] Instituto de Física de Cantabria (CSIC-Universidad de Cantabria), Avda. de los Castros s/n, Santander, Spain
[57] Jet Propulsion Laboratory, California Institute of Technology, 4800 Oak Grove Drive, Pasadena, CA, USA
[58] Jodrell Bank Centre for Astrophysics, Alan Turing Building, School of Physics and Astronomy, The University of Manchester, Oxford Road, Manchester, M13 9PL, UK
[59] Kavli Institute for Cosmology Cambridge, Madingley Road, Cambridge, CB3 0HA, UK
[60] LAL, Université Paris-Sud, CNRS/IN2P3, Orsay, France
[61] LERMA, CNRS, Observatoire de Paris, 61 avenue de l'Observatoire, Paris, France
[62] Laboratoire AIM, IRFU/Service d'Astrophysique – CEA/DSM – CNRS – Université Paris Diderot, Bât. 709, CEA-Saclay, 91191 Gif-sur-Yvette Cedex, France
[63] Laboratoire Univers et Théories (LUTh), UMR 8102 CNRS, Observatoire de Paris, Université Paris Diderot, 5 place Jules Janssen, 92190 Meudon, France
[64] Laboratoire de Physique Subatomique et de Cosmologie, Université Joseph Fourier Grenoble I, CNRS/IN2P3, Institut National Polytechnique de Grenoble, 53 rue des Martyrs, 38026 Grenoble Cedex, France
[65] Laboratoire de Physique Théorique, Université Paris-Sud 11 & CNRS, Bâtiment 210, 91405 Orsay, France
[66] Max-Planck-Institut für Astrophysik, Karl-Schwarzschild-Str. 1, 85741 Garching, Germany
[67] McGill Physics, Ernest Rutherford Physics Building, McGill University, 3600 rue University, Montréal, QC, H3A 2T8, Canada
[68] National University of Ireland, Department of Experimental Physics, Maynooth, Co. Kildare, Ireland
[69] Niels Bohr Institute, Blegdamsvej 17, Copenhagen, Denmark
[70] Optical Science Laboratory, University College London, Gower Street, London, UK
[71] SB-ITP-LPPC, EPFL, 1015 Lausanne, Switzerland
[72] SISSA, Astrophysics Sector, via Bonomea 265, 34136 Trieste, Italy
[73] School of Physics and Astronomy, Cardiff University, Queens Buildings, The Parade, Cardiff, CF24 3AA, UK
[74] School of Physics and Astronomy, University of Nottingham, Nottingham NG7 2RD, UK
[75] Space Sciences Laboratory, University of California, Berkeley, CA, USA
[76] Special Astrophysical Observatory, Russian Academy of Sciences, Nizhnij Arkhyz, Zelenchukskiy region, 369167 Karachai-Cherkessian Republic, Russia
[77] Sub-Department of Astrophysics, University of Oxford, Keble Road, Oxford OX1 3RH, UK
[78] Theory Division, PH-TH, CERN, 1211, Geneva 23, Switzerland
[79] UPMC Univ Paris 06, UMR7095, 98bis boulevard Arago, 75014 Paris, France
[80] Université de Toulouse, UPS-OMP, IRAP, 31028 Toulouse Cedex 4, France
[81] University of Granada, Departamento de Física Teórica y del Cosmos, Facultad de Ciencias, Granada, Spain
[82] University of Granada, Instituto Carlos I de Física Teórica y Computacional, Granada, Spain
[83] Warsaw University Observatory, Aleje Ujazdowskie 4, 00-478 Warszawa, Poland

Pages 20 to 25 are available in the electronic edition of the journal at http://www.aanda.org

Appendix A: Implementation in RECFAST

The recombination equations form a set of three differential equations for the proton fraction $x_p = n_p/n_{\rm H}$, the singly ionized helium fraction $x_{\rm HeII} = n_{\rm HeII}/n_{\rm H}$ and the matter temperature $T_{\rm M}$. The electron fraction is then obtained from electric neutrality as $x_{\rm e} = x_p + x_{\rm HeII}$. Following Seager et al. (1999), Seager et al. (2000), and Wong et al. (2008), these are given by

$$\frac{{\rm d}x_p}{{\rm d}z} = \frac{C_{\rm H}}{H_0(1+z)E(z)}\left[x_{\rm e}x_{\rm p}n_{\rm H}\widetilde{\alpha}_{\rm H} - \beta_{\rm H}(1-x_{\rm p})\,{\rm e}^{-h\nu_{\rm H2s}/kT_{\rm M}}\right] \tag{A.1}$$

$$\begin{aligned}\frac{{\rm d}x_{\rm HeII}}{{\rm d}z} = {}& \frac{C_{\rm HeI}}{H_0(1+z)E(z)}\left[x_{\rm e}x_{\rm HeII}n_{\rm H}\widetilde{\alpha}_{\rm HeI}\right.\\ & \left.-\beta_{\rm HeI}(f_{\rm He}-x_{\rm HeII})\,{\rm e}^{-h\nu_{\rm HeI,2^1s}/kT_{\rm M}}\right]\\ & + \frac{C^{\rm t}_{\rm HeI}}{H_0(1+z)E(z)}\left[x_{\rm e}x_{\rm HeII}n_{\rm H}\widetilde{\alpha}^{\rm t}_{\rm HeI}\right.\\ & \left.-\frac{g_{\rm HeI,2^3s}}{g_{\rm HeI,1^1s}}\beta^{\rm t}_{\rm HeI}(f_{\rm He}-x_{\rm HeII})\,{\rm e}^{-h\nu_{\rm HeI,2^3s}/kT_{\rm M}}\right],\end{aligned} \tag{A.2}$$

$$\frac{{\rm d}T_{\rm M}}{{\rm d}z} = \frac{8\sigma_{\rm T}a_{\rm R}T^4}{3H_0E(z)(1+z)m_{\rm e}c}(T_{\rm M}-T) + \frac{2T_{\rm M}}{1+z}, \tag{A.3}$$

where the second term of Eq. (A.2) accounts for recombination through the triplets, via the semi-forbidden transition $2^3{\rm p} \rightarrow 1^1{\rm s}$. Here T is the radiation temperature that evolves as $T = T_0(1+z)$.

Equations (A.1)–(A.3) involve quantities that remain constant due to our choice of units, such as the speed of light c, the *Planck* constant h and the radiation constant $a_{\rm R} = 4\pi^2k^4/(6\pi c^3\hbar^3)$. They also involve spectroscopic quantities, such as the hydrogen 2s–1s frequency $\nu_{\rm H2s}$, and the helium $2^1{\rm p}$–$1^1{\rm s}$ and $2^3{\rm p}$–$1^1{\rm s}$ frequencies, $\nu_{\rm HeI,2^1s}$ and $\nu_{\rm HeI,2^3s}$. All these frequencies scale as $\alpha^2 m_{\rm e}$, as already described in Sect. 2.1. The importance of these rates on the CMB spectrum has been emphasized recently by Mukhanov et al. (2012). The coefficients C are explicitly given by

$$C_{\rm H} = \frac{1 + K_{\rm H}\Lambda_{\rm H}n_{\rm H}(1-x_{\rm p})}{1 + K_{\rm H}(\Lambda_{\rm H}+\beta_{\rm H})n_{\rm H}(1-x_{\rm p})}, \tag{A.4}$$

$$C_{\rm HeI} = \frac{1 + K_{\rm HeI}\Lambda_{\rm HeI}n_{\rm H}(f_{\rm He}-x_{\rm HeII})\,{\rm e}^{h\nu_{\rm ps}/kT_{\rm M}}}{1 + K_{\rm HeI}(\Lambda_{\rm He}+\beta_{\rm HeI})n_{\rm H}(f_{\rm He}-x_{\rm HeII})\,{\rm e}^{h\nu_{\rm ps}/kT_{\rm M}}}, \tag{A.5}$$

$$C^{\rm t}_{\rm HeI} = \frac{1}{1 + K^{\rm t}_{\rm HeI}\beta^{\rm t}_{\rm HeI}n_{\rm H}(f_{\rm He}-x_{\rm HeII})\,{\rm e}^{h\nu^{\rm t}_{\rm ps}/kT_{\rm M}}}. \tag{A.6}$$

These involve the H 2s–1s and He I $2^1{\rm s}$–$1^1{\rm s}$ two-photon decay rates, $\Lambda_{\rm H}$ and $\Lambda_{\rm HeI}$, which both scale as $\alpha^8 m_{\rm e}$.

We also need the case B recombination coefficient for hydrogen (also by unfortunate convention called α), which we label $\widetilde{\alpha}_{\rm H}$, and the two recombination coefficients for helium, $\widetilde{\alpha}_{\rm HeI}$ (singlet) and $\widetilde{\alpha}^{\rm t}_{\rm HeI}$ (triplet), which are fitted by the same functional form given in Péquignot et al. (1991). These are all assumed to scale as $\alpha^3 m_{\rm e}^{-3/2}$ (see footnote 2 for further discussion on this dependence). The photoionization coefficients $\beta_{\rm H}$ and $\beta_{\rm HeI}$ are given by $\beta_{\rm i} = \widetilde{\alpha}_{\rm i}(2\pi m_{\rm e}kT_{\rm M}/h^2)^{3/2}\exp(-h\nu_{\rm i}/kT_{\rm M})$, so that they scale mostly as the recombination coefficients, up to the dependence induced by the frequency in the exponential factor.

The "K-quantities", $K_{\rm H}$, $K_{\rm HeI}$ and $K^{\rm t}_{\rm HeI}$, are, respectively, the cosmological redshifting of the hydrogen Lyman-α and helium $2^1{\rm p}$–$1^1{\rm s}$ and $2^3{\rm p}$–$1^1{\rm s}$ transition lines. It can be shown that they scale as $\alpha^{-6}m_{\rm e}^{-3}$.

More details on the physical constant dependence of these equations can be found in Kaplinghat et al. (1999), Battye et al. (2001), Scoccola (2009), and Narimani et al. (2012).

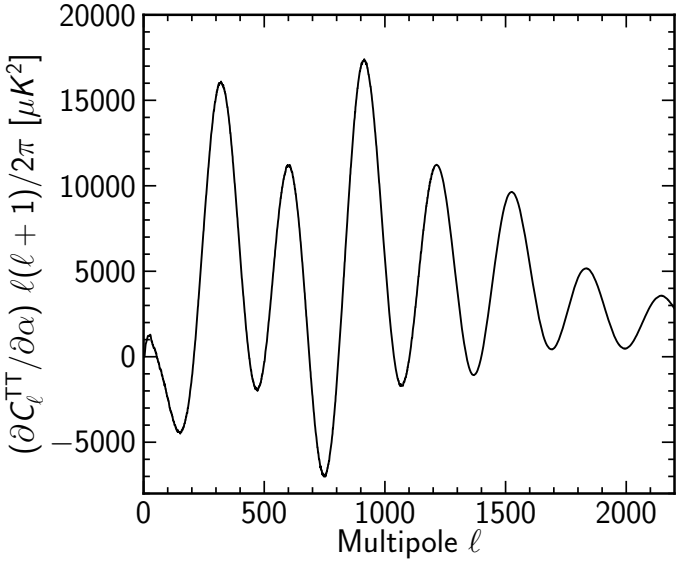

Fig. A.1. The quantity $\partial C_\ell^{TT}/\partial\alpha$, assuming the *Planck* best-fit model cosmological parameters.

Appendix B: How α and $m_{\rm e}$ affect the power spectrum

In this Appendix, we illustrate how α and $m_{\rm e}$ affect the CMB power spectra through the different terms listed in Sect. 2.1. The dependences described here have already been discussed in earlier papers (Hannestad 1999; Kaplinghat et al. 1999; Battye et al. 2001). However, we are interested in addressing the following two specific questions.

The first aims to identify the quantities in Sect. 2.1 whose change, due to a variation of the constants, gives the strongest effect on the CMB power spectra.

The second aims to understand what are the dependences that determine the different behaviour of the angular power spectra under a variation of α or $m_{\rm e}$.

In order to investigate these two issues, we perform the following exercise. We add a variation of α (or $m_{\rm e}$) only to one or a few terms at a time, while keeping the value of the constants at the standard values in all other terms. We consider the following cases:

1. variation only in the hydrogen binding energy, as in Eq. (8);
2. variation only in the energy of the "Lyman-α" (Ly α) transition (here improperly defined as the average of the (2s-continuum) and (2p-continuum) energy levels);
3. variation only in the previous two terms together;
4. variation of the previous two terms and the Thomson scattering cross-section $\sigma_{\rm T}$, as in Eq. (6);
5. variation only in the previous three terms and the 2-photon decay rate $\Lambda_{\rm i}$, as in Eq. (13);
6. variation of all the terms where the constants appear.

We test the effects on the CMB angular power spectra of the sequence of cases listed above, both for variations of α and $m_{\rm e}$, and

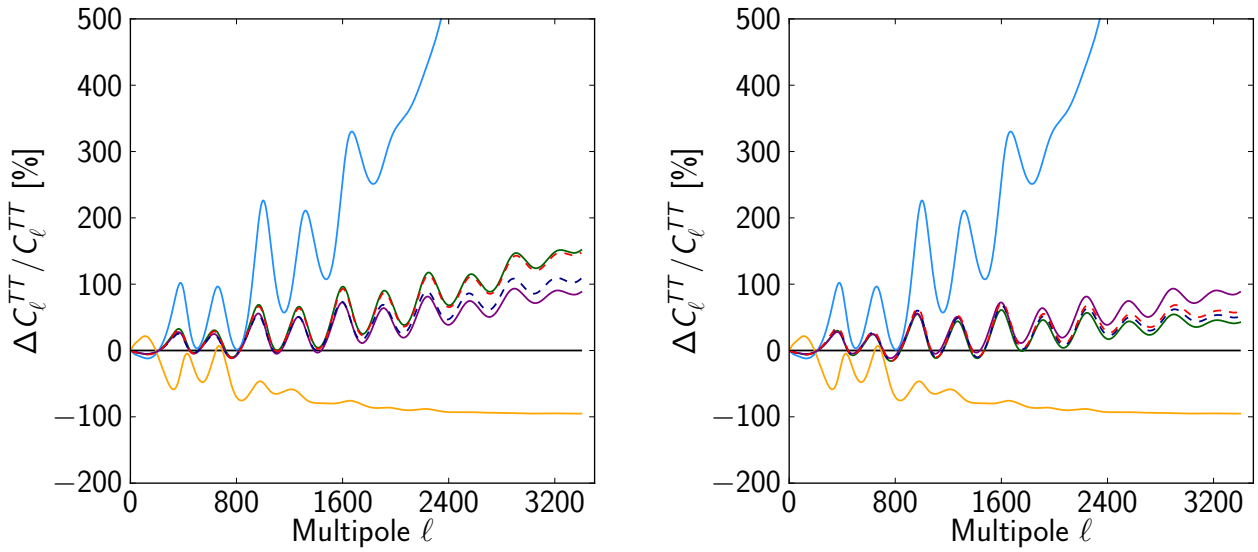

Fig. B.1. *Left*: relative difference between the CMB TT power spectrum calculated using a value of α/α_0 different from unity (in one, a few or all the terms where it appears), and a power spectrum, $C_{\ell,\rm st}$, calculated using a standard value of $\alpha/\alpha_0 = 1$. We thus plot $\Delta C_\ell/C_\ell = (C_\ell - C_{\ell,\rm st})/C_{\ell,\rm st}$[%]. The cases considered are α varying: only in the hydrogen binding energy (solid light blue); only in the Ly α energy (solid yellow); in both the previous two terms (solid purple); in both the previous terms and in the Thomson scattering cross-section (dashed dark blue); in the previous three terms and in the 2−photon decay rate (dashed red); and in all terms (solid green). In each case, we assume that α varies by +5% ($\alpha/\alpha_0 = 1.05$) only in the terms considered, while it is $\alpha/\alpha_0 = 1$ in all the others. *Right*: same as the cases on the left, but for a variation of $m_{\rm e}$ of 10% ($m_{\rm e}/m_{\rm e0} = 1.1$).

show the results in Fig. B.1. There we plot the relative difference between: (i) the angular power spectrum obtained assuming that α (or $m_{\rm e}$) is changing only in a few terms as listed above; and (ii) the standard angular power spectrum, with the constants set to their usual values. For α we assume a variation at the 5% level, while for $m_{\rm e}$ we assume a variation at the 10% level. This latter choice is motivated by the fact that atomic energies scale as $\alpha^2 m_{\rm e}$. Hence changing $m_{\rm e}$ by twice the α change should result in similar effects on the angular power spectra, making the comparison between the effects on spectra easier. This is what is shown in Fig. B.1: the blue line (relative to the change of hydrogen binding energy only, item 1 in the list), the yellow line (relative to a change in the Ly α energy level only; item 2) and the purple line (sum of the previous two effects, item 3) are identical for α and for $m_{\rm e}$.

It is evident from the figures that the major contribution to the change in the angular power spectrum induced by a variation of α or $m_{\rm e}$ comes from the change in the hydrogen binding energy (item 1) and Ly α energy (item 2). The main effect of changing these two energy levels is to modify the hydrogen 2s–1s transition energy, $h\nu_{\rm H2s}$, in Eq. (A.1), since this is, by definition, the difference between the first two mentioned energies. Increasing $h\nu_{\rm H2s}$ through, e.g., an increase of the hydrogen binding energy, weakens the ionization term in Eq. (A.1) through a decrease of the Boltzmann factor $\mathrm{e}^{-h\nu_{\rm H2s}/kT_{\rm M}}$, resulting in earlier recombination. As a consequence, acoustic peaks move to higher multipoles, early ISW is increased and the Silk damping is decreased, so that the overall amplitude of the peaks is increased, as already described in Sect. 2.1. On the other hand, increasing the Ly α energy has the opposite effect on $h\nu_{\rm H2s}$ and would thus tend to delay recombination. However, this effect is mitigated by the other terms where the Ly α energy level appears, such as in the K factors encoding the redshifting of the Ly α photons in Eqs. (12) and (A.4). This is why the effects of increasing both the hydrogen binding energy and the Ly α energy, through an increase of the value of the constants, do not perfectly cancel, but the first effect dominates over the second. Furthermore, as already mentioned, these effects are qualitatively the same for α and for $m_{\rm e}$, although of different magnitude.

A distinction in the effects of α or $m_{\rm e}$ is, however, introduced if we now also consider the impact on the Thomson scattering cross-section $\sigma_{\rm T}$ (item 4). As already described in Sect. 2.1, $\sigma_{\rm T} \propto \alpha^2/m_{\rm e}^2$, i.e., an increase in the value of α increases $\sigma_{\rm T}$, while an increase in $m_{\rm e}$ decreases $\sigma_{\rm T}$. Consequently, an increase in $\sigma_{\rm T}$ increases Silk damping, while a decrease in $\sigma_{\rm T}$ decreases Silk damping. This is the reason why adding the effect of the constants on the Thomson cross-section, shown in the dark-blue dashed lines in Fig. B.1, increases the amplitude of the peaks for a larger value of α, while it decreases it for a larger value of $m_{\rm e}$. Consequently, this is the reason why α and $m_{\rm e}$ have different effects on the amplitude of the peaks.

We now analyse the effect of adding the variation of constants in the 2-photon decay rate (item 5). As shown in Eq. (13), this ratio depends much more strongly on α than on $m_{\rm e}$, $\Lambda \propto \alpha^8 m_{\rm e}$. The effect of increasing the value of the constants in this term is again to shift recombination to earlier times, but, as expected, the impact is much larger when varying α than when varying $m_{\rm e}$, as shown by the dashed red line in Fig. B.1. Finally, adding the variation of the constants in all the remaining terms, including the equations for helium recombination, further adjusts the amplitudes at the few percent level, to finally converge to the green solid line. In particular, we verified that neglecting the effects of the variation of the constants on helium recombination impacts the constraints by less than 5%.

For the sake of completeness, we show in Fig. B.2 the effect of varying the constants on the EE-polarization. The effects are similar to the ones described for temperature, although changes are in this case even larger. High accuracy observations of the polarization power spectra might therefore help in improving the constraints on fundamental constants.

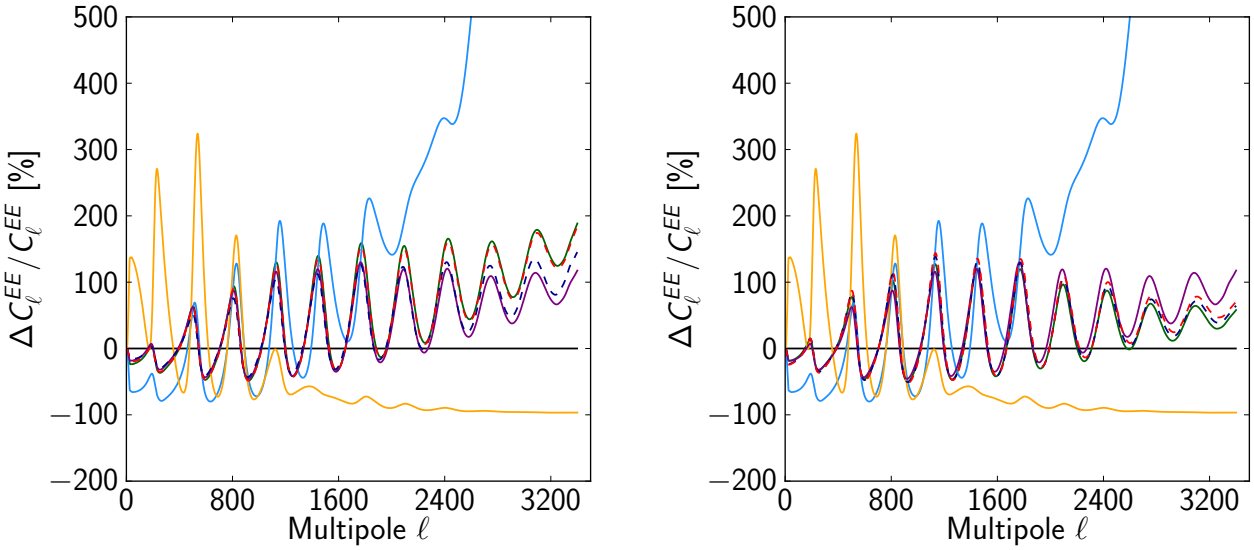

Fig. B.2. Same as Fig. B.1, but for EE polarization power spectra.

Appendix C: Additional tables and figures

In this Appendix, we collect some of the tables and figures already extensively described in the paper. We show the constraints on cosmological parameters for a ΛCDM+α + $N_{\rm eff}$ model in Table C.1, a ΛCDM+α + Y_p model in Table C.2, a ΛCDM+α removing the low-ℓ data in Table C.3, and for a ΛCDM+$m_{\rm e}$ model removing the low-ℓ data in Table C.4. Furthermore, Fig. C.1 shows the two-dimensional contour plots between α and foreground parameters, while Fig. C.2 shows the same for $m_{\rm e}$.

Table C.1. Constraints on the cosmological parameters for the base ΛCDM model with the addition of a varying fine structure constant and number of relativistic species, $N_{\rm eff}$.

Parameter	*Planck*+WP 68% limits	*Planck*+WP+highL 68% limits	WMAP-9 68% limits
$\Omega_{\rm b}h^2$	$0.02204^{+0.00052}_{-0.00061}$	0.02229 ± 0.00054	$0.0230^{+0.0012}_{-0.0010}$
$\Omega_{\rm c}h^2$	$0.1174^{+0.0088}_{-0.012}$	$0.1227^{+0.0088}_{-0.013}$	$0.140^{+0.024}_{-0.044}$
H_0	$65.2^{+5.8}_{-8.1}$	$69.0^{+6.0}_{-8.0}$	79^{+20}_{-9}
τ	$0.095^{+0.014}_{-0.016}$	$0.095^{+0.014}_{-0.016}$	0.089 ± 0.014
$N_{\rm eff}$	$3.04^{+0.54}_{-0.73}$	$3.30^{+0.53}_{-0.76}$	$4.46^{+1.5}_{-2.4}$
α/α_0	$0.9933^{+0.0073}_{-0.0083}$	$0.9988^{+0.0067}_{-0.0075}$	$1.006^{+0.020}_{-0.016}$
$n_{\rm s}$	0.974 ± 0.017	0.971 ± 0.017	0.989 ± 0.026
$\ln(10^{10}A_{\rm s})$	3.105 ± 0.035	$3.107^{+0.034}_{-0.038}$	$3.130^{+0.075}_{-0.063}$

Notes. We quote 68% CL errors.

Table C.2. Constraints on the cosmological parameters for the base ΛCDM model with the addition of a varying fine structure constant and helium abundance, Y_p.

Parameter	*Planck*+WP 68% limits	*Planck*+WP+highL 68% limits	WMAP-9 68% limits
$\Omega_b h^2$	$0.02220^{+0.00073}_{-0.0013}$	$0.02245^{+0.00075}_{-0.0014}$	0.0232 ± 0.0014
$\Omega_c h^2$	$0.1179^{+0.0051}_{-0.0063}$	$0.1202^{+0.0057}_{-0.0069}$	$0.1166^{+0.0061}_{-0.0079}$
H_0	$66.6^{+6.2}_{-12}$	$69.8^{+6.1}_{-13}$	75 ± 10
τ	$0.095^{+0.014}_{-0.016}$	$0.094^{+0.013}_{-0.016}$	$0.088^{+0.013}_{-0.015}$
Y_p	<0.306	<0.325	<0.345
α/α_0	$0.996^{+0.015}_{-0.024}$	$1.003^{+0.014}_{-0.026}$	1.010 ± 0.023
n_s	0.976 ± 0.013	0.968 ± 0.012	0.976 ± 0.015
$\ln(10^{10} A_s)$	3.107 ± 0.030	3.102 ± 0.028	3.096 ± 0.039

Notes. We quote 68% CL errors.

Table C.3. Constraints on the cosmological parameters for the base ΛCDM model with the addition of a varying fine structure constant for *Planck* data, removing the low-ℓ multipoles and placing a Gaussian prior on τ.

Parameter	*Planck*−low l+τ prior 68% limits	*Planck*−low l+τ prior+highL 68% limits
$\Omega_b h^2$	0.02194 ± 0.00028	0.02194 ± 0.00028
$\Omega_c h^2$	0.1205 ± 0.0040	0.1228 ± 0.0038
H_0	65.6 ± 1.9	66.6 ± 1.7
τ	0.094 ± 0.013	0.093 ± 0.012
α/α_0	0.9970 ± 0.0054	1.0011 ± 0.0045
n_s	0.961 ± 0.016	0.948 ± 0.015
$\ln(10^{10} A_s)$	3.105 ± 0.026	3.101 ± 0.025

Notes. We quote 68% CL errors.

Table C.4. Constraints on the cosmological parameters for the base ΛCDM model with the addition of the mass of the electron for *Planck* data, removing the low-ℓ multipoles and placing a Gaussian prior on τ.

Parameter	*Planck*−low l+τ prior 68% limits	*Planck*−low l+τ prior+highL 68% limits
$\Omega_b h^2$	$0.0221^{+0.0023}_{-0.0019}$	$0.0220^{+0.0017}_{-0.0021}$
$\Omega_c h^2$	$0.123^{+0.011}_{-0.012}$	0.1224 ± 0.0098
H_0	...	<76.1
τ	0.092 ± 0.012	0.094 ± 0.012
m_e/m_{e0}	$1.007^{+0.099}_{-0.081}$	1.001 ± 0.075
n_s	0.9527 ± 0.0082	0.9503 ± 0.0081
$\ln(10^{10} A_s)$	3.101 ± 0.026	3.102 ± 0.025

Notes. We quote 68% CL errors. In this case we find that the Hubble parameter is unconstrained within the uniform prior we set, i.e., $40 < (H_0/\mathrm{km\,s^{-1}\,Mpc^{-1}}) < 100$.

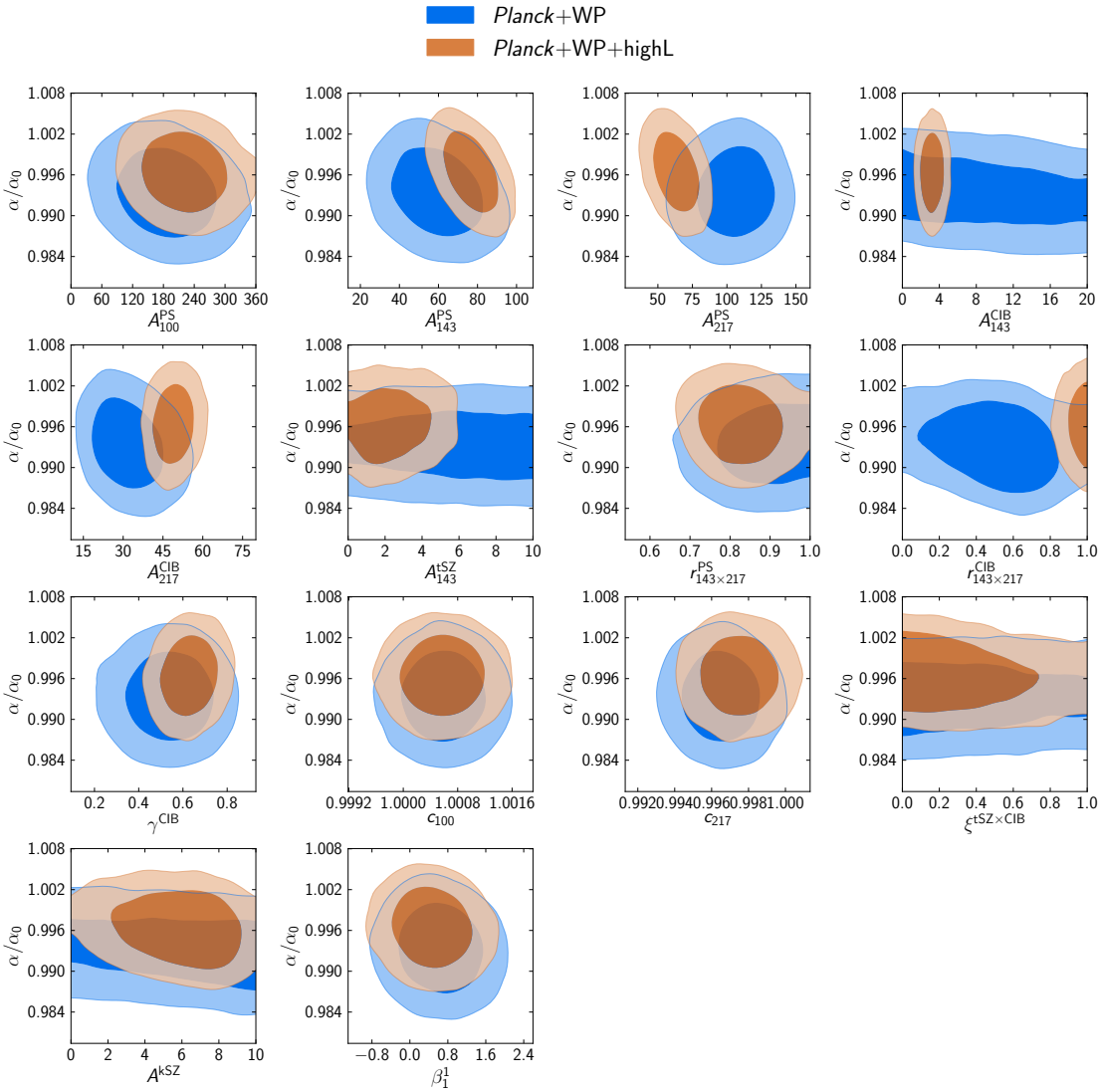

Fig. C.1. Two-dimensional likelihood contours (68% and 95%) for α/α_0 versus different foreground/beam/calibration parameters, as defined in Table 4 of Planck Collaboration XVI (2014). We show results for *Planck*+WP (blue) and *Planck*+WP+highL (orange) data combinations.

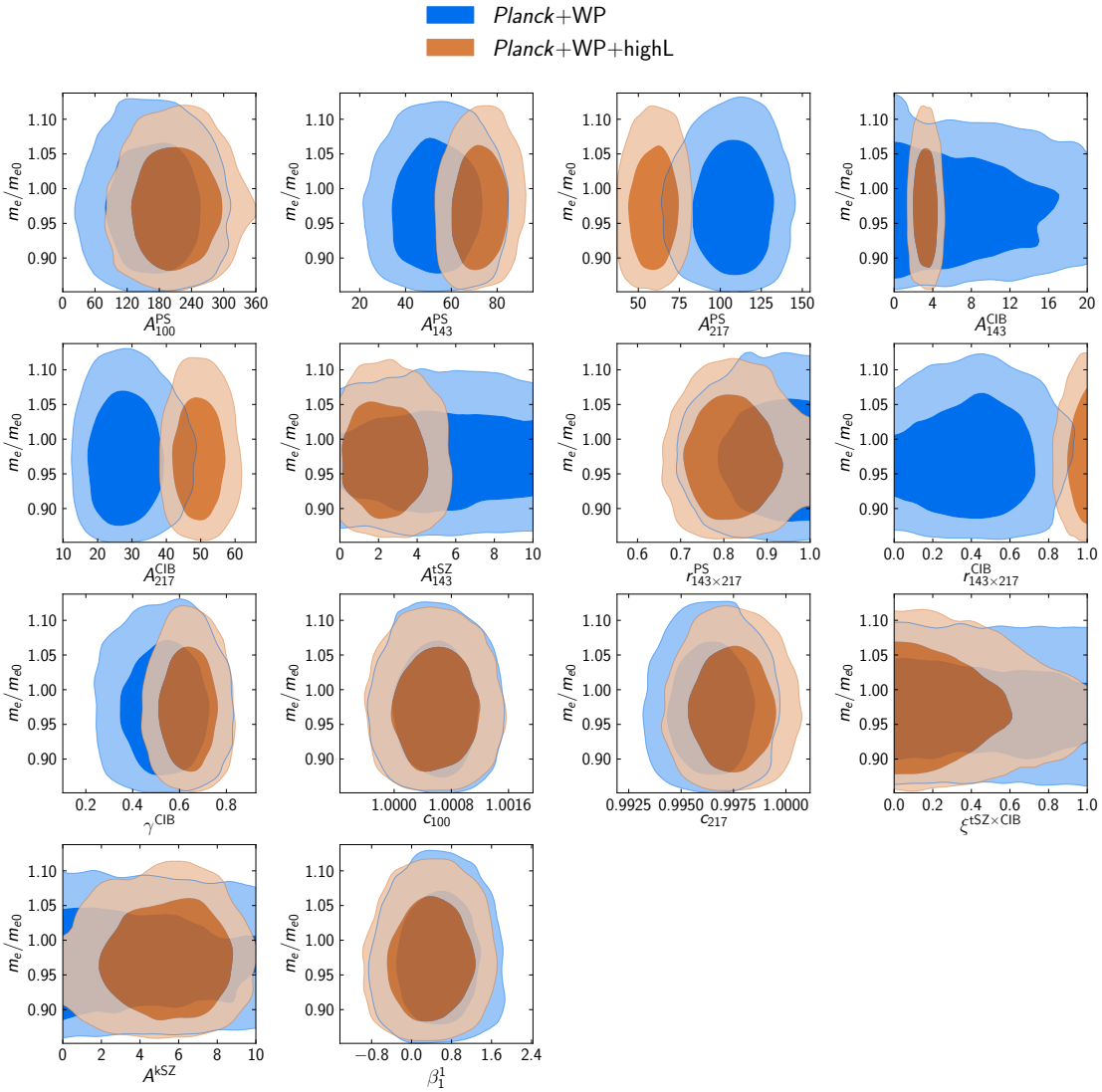

Fig. C.2. Two-dimensional likelihood contours (68% and 95%) for m_e/m_{e0} versus different foreground/beam/calibration parameters, as defined in Table 4 in Planck Collaboration XVI (2014). We show results for *Planck*+WP (blue) and *Planck*+WP+highL (orange) data combinations.